Tropospheric N$_2$O Variability

H. LEVY II, J. D. MAHLMAN, AND W. J. MOXIM

Geophysical Fluid Dynamics Laboratory/NOAA, Princeton University, Princeton, New Jersey 08540

Tropospheric N$_2$O climatologies are simulated with the GFDL general circulation/tracer model for three idealized source specifications: (1) a constant surface flux of 1.44×10^9 molecules cm^{-2} s^{-1} distributed uniformly over the earth's surface with a global source strength of 17 tg N$_2$O yr^{-1} and an atmospheric lifetime of 131 yr; (2) a 13 month integration of the stable N$_2$O field from experiment 1 with its N$_2$O source removed; (3) a constant surface flux of 2.24×10^{10} molecules cm^{-2} s^{-1} over only those land areas with precipitation in excess of an arbitrary limit of 127 cm yr^{-1}, but with the same global strength (17 tg N$_2$O yr^{-1}) and atmospheric lifetime (131 yr) as in experiment 1. In the boundary layer the model produces an interhemispheric gradient with a minimum in the northern hemisphere (N.H.). This is due to the greater downward transport in the N.H. which results in more dilution of N.H. boundary layer N$_2$O mixing ratios by the N$_2$O poor air from the lower stratosphere. The boundary layer distribution of N$_2$O is also influenced by the distribution of the surface source. The lack of an N$_2$O maximum in the model's N.H. boundary layer suggests that, unlike the model's idealized source, the true source has a large excess in the northern hemisphere. Above the boundary layer the north-south gradient is controlled by the large-scale vertical transport which produces a N.H. minimum in N$_2$O mixing ratio. The impact of the surface source distribution is small. Current measurements at 500 mbar have too low a precision to confirm or disprove the model prediction of an interhemispheric gradient with a N.H. minimum in the middle troposphere. The sources of temporal variability in the model's N$_2$O fields are transient motions of all scales acting on mixing ratio gradients, both vertical and horizontal. The model finds that a small surface source of 17 tg N$_2$O yr^{-1}, sufficient to balance stratospheric destruction, is more than able to maintain the observed variability in the boundary layer ($\leq 1.0\%$). The empirical Junge rule relating temporal relative standard deviation to lifetime clearly does not apply to measurements in the boundary layer. There, the variability is dependent on local meteorology and source strength rather than on atmospheric lifetime. It ranges from $<0.1\%$ in regions far from any source to $1.0–2.0\%$ in regions with both a source and weak vertical motion. However, the measurement of local mixing ratio time series in the boundary layer, when combined with local meteorological data, should give considerable information about the surrounding sources.

1. INTRODUCTION

N$_2$O was first observed in the earth's atmosphere by *Adel* [1939] who later proposed a bacterial source in the soil [*Adel*, 1951]. Its oxidation in the stratosphere by O(^{1}D) is the major natural source of stratospheric NO [*Crutzen*, 1971; *McElroy and McConnell*, 1971; *Nicolet and Vergison*, 1971] which is thought to drive the dominant destruction cycle for stratospheric O$_3$ [*Crutzen*, 1970].

In the recent past there has been considerable interest in the possible increase of stratospheric N$_2$O due to man's activities. Both the nitrogen fertilizer source [*Crutzen*, 1976; *Liu et al.*, 1976; *McElroy et al.*, 1977] and the combustion source [*Weiss and Craig*, 1976; *Pierotti and Rasmussen*, 1976] have been of concern. The impact of these anthropogenic sources depends on the size and distribution of the natural sources and sinks of N$_2$O in the troposphere.

When we began this work in 1976 there was considerable uncertainty regarding the size of tropospheric sources, the existence as well as the size of tropospheric sinks, and the magnitude of tropospheric variability of N$_2$O. Using boundary layer measurements of N$_2$O and an empirical formula relating temporal relative standard deviation to atmospheric lifetime, *Junge* [1974] estimated a short lifetime (8–12 yr) which implied a large tropospheric source. This view of N$_2$O as a trace constituent with a relatively large source, short lifetime, and high variability was summed up in a review

paper by *Hahn and Junge* [1977]. An intermediate position was presented by *McElroy et al.* [1976] who concluded that N$_2$O had a relatively short lifetime (10–20 years) and proposed bacterial consumption of N$_2$O in the ocean as an additional sink. On the other hand, there were some preliminary measurements (R. F. Weiss, private communication, 1976) which supported a much lower variability. This uncertain state was represented by *Liu et al.* [1977] who concluded that nothing regarding tropospheric sources, sinks, and lifetimes of N$_2$O was certain.

Since the actual tropospheric N$_2$O source function was not known, we chose to construct a series of idealized source experiments. They were based on the two properties of N$_2$O which were well proven and precisely calculable: its stratospheric destruction by photodissociation and O(^{1}D) oxidation and its production by a net surface source which balanced that destruction. We wished to determine the level of tropospheric temporal and spatial variability supported by such a small source, the sources of this variability, and its connection to atmospheric lifetime. The experiments were designed to determine the effect of source strength and spatial variability on the spatial and temporal behavior of N$_2$O in the troposphere. They were not meant to provide an exact simulation of the actual tropospheric N$_2$O climatology but were meant to establish bounds for it.

In the first experiment the surface source was spread uniformly throughout the globe. While this distribution was not expected to be realistic, it removed spatial inhomogeneity of the source as a cause of model N$_2$O variability. The experiment allowed us to focus on variability caused by transport. In the second experiment the stable N$_2$O field

TABLE 1. N₂O Destruction Chemistry

Equation Number	Equation	Rate Coefficient	Reference
R1	$O_2 + h\nu \rightarrow 2O$		*Ackerman* [1971]
R2	$O_3 + h\nu \rightarrow O(^1D) + O_2$		*Ackerman* [1971] and quantum yields from *Levy* [1974]
R3	$O_3 + h\nu \rightarrow O(^3P) + O_2$	$J3 = 7.6 \times 10^{-4*}$	*Ackerman* [1971]
R4	$N_2O + h\nu \rightarrow N_2 + O$	$J4 = 4.6 \times 10^{-8*}$	*Johnston and Selwyn* [1975]
R5	$O(^1D) + N_2O \rightarrow N_2 + O_2$ or 2NO	$K5 = 2.2 \times 10^{-10\dagger}$	*Hampson and Garvin* [1975]
R6	$O(^1D) + O_2 \rightarrow O(^3P) + O_2$	$K6 = 7.4 \times 10^{-11\dagger}$	*Hampson and Garvin* [1975]
R7	$O(^1D) + N_2 \rightarrow O(^3P) + N_2$	$K7 = 5.4 \times 10^{-11\dagger}$	*Hampson and Garvin* [1975]

*Daytime average for July, 0° latitude, and 10 mbar (s^{-1}).
†Units are cm^3 molecule^{-1} s^{-1}.

from the first experiment was integrated for 13 months with no source. This was done to determine the contribution of the source and the resulting surface accumulation to tropospheric variability. A third experiment with the same global source strength, but distributed only over wet land, demonstrated the contribution of source spatial variability to the variability of N₂O. Preliminary results of these three experiments have already been published [*Levy et al.*, 1979; *Levy and Mahlman*, 1980].

Between the start of these experiments in 1976 and their detailed analysis in 1980, significant new data on tropospheric N₂O has emerged. These recent developments are reviewed by *McElroy* [1980] and *Levy and Mahlman* [1980].

The current view of tropospheric N₂O can now be summarized as low variability, a variety of small natural soil and water sources that should be sufficient to balance stratospheric destruction, and the possibility of dust and sand surface destruction. There is still the question of the actual magnitudes of the soil and water sources as well as the question of the existence and magnitude of a dust or sand sink. With these three numerical experiments we will demonstrate that a stratospheric sink balanced by a small surface source is sufficient to explain the global structure and variability, both in time and space, of the N₂O distribution as we now understand it. With the help of the model's results, we will also identify some key tropospheric N₂O measurements that should be undertaken.

2. Model Description

All three numerical experiments employed the GFDL general circulation/tracer model. This model has already been used to study the global dispersion and rainout of radioactive debris from an idealized nuclear weapons test [*Mahlman and Moxim*, 1978] and the 3-D structure and behavior of a simplified ozone tracer [*Mahlman et al.*, 1980]. This model has 11 terrain following (σ) surfaces in the vertical with standard heights of 31.4, 22.3, 18.8, 15.5, 12.0, 8.7, 5.5, 3.1, 1.5, 0.5, and 0.08 km and a horizontal grid size of approximately 265 km. The continuity equation for the volume mixing ratio of a given trace constituent (R) is evaluated by the method of finite differences. This equation, in σ coordinates, is given by

$$\frac{\partial Rp_*}{\partial t} = -\nabla_\sigma \cdot \vec{V}_2 p_* R - \frac{\partial}{\partial \sigma} \dot{\sigma} p_* R$$

$$+ \text{DIFFUSION} + \text{SO } p_* - D R p_* \quad (1)$$

where p_* is surface pressure, $\vec{V}_2$ is the horizontal wind vector, $\dot{\sigma}$ is the vertical motion in σ coordinates, SO is the source of R, and D is the first order destruction rate coefficient (s^{-1}) of R. The contribution from DIFFUSION (parameterized subgrid-scale vertical and horizontal diffusion) is discussed in 2.1. The wind fields used in (1) are the 6 hour time averaged wind fields generated by a GFDL general circulation model [*Manabe et al.*, 1974]. This general circulation model has no diurnal physics and does not have adequate spatial resolution to simulate realistic atmospheric fluctuations on time scales shorter than 1 day. The preparation of the input data, the relevant features of the general circulation model providing it, and the numerical techniques used to integrate (1) have all been described previously [*Mahlman and Moxim*, 1978].

2.1 Transport.

The calculation of $\nabla_\sigma \cdot \vec{V}_2 p_* R$ and $(\partial/\partial\sigma) \dot{\sigma} p_* R$ has been described in an earlier paper [*Mahlman and Moxim*, 1978]. While that paper also contained an extensive discussion of subgrid-scale diffusion, the treatment of DIFFUSION in these experiments is different. For horizontal diffusion, we retained the scheme of *Mahlman and Moxim* [1978], but changed the arbitrary scale selectivity constant Q. In the vertical we added a diffusion coefficient which depends upon a moist Richardson number.

The impact of these subgrid-scale diffusion parameterizations on variability was examined, in a separate experiment, by increasing both horizontal and vertical subgrid-scale diffusion to values which equaled or exceeded realistic physical upper limits. While this very high subgrid-scale diffusion resulted in a 25–30% reduction in variability, it did not significantly effect the relationship between source structure and N₂O variability. Thus, even with these unrealistically high levels of subgrid-scale diffusion, most of the tropospheric N₂O variability remained. For details of these schemes and the choices for the parameter study, see Appendix A.

2.2 Destruction.

The chemical reactions and rate coefficients needed to calculate N₂O stratospheric destruction are given with relevant references in Table 1. The destruction rate coefficient used in (1) is given, for a particular latitude belt and vertical level, by

$$D = C \cdot \left(\frac{J_2 R_{O_3}}{0.79K7 + 0.21K6} K5 \right) \quad (2)$$

R_{O_3}, the yearly mean O_3 mixing ratio for a given latitude and height, is taken from observed data as described by *Fels et al.* [1980]. The coefficient C is a precalculated factor that corrects for the coarse vertical resolution in the model middle stratosphere as well as the nonlinear behavior of the J's and the N_2O mixing ratio in that region. A detailed discussion of C is given in Appendix B.

In keeping with the finite difference nature of the numerical model, we calculated the photodissociation rate coefficient for species I at a given level K by

$$J(\lambda) = J_1(\lambda)J_2(\lambda)J_3(\lambda)/(R_I(K)n_K)$$

where

$$J_1(\lambda) = \frac{\sigma_I(\lambda)R_I(K)}{\sum_i \sigma_i(\lambda)R_i(K)}$$

$$J_2(\lambda) = \left(1 - \exp - \left[\sec\chi \, n_K \sum_i \sigma_i(\lambda)R_i(K)\right]\right) \quad (3)$$

$$J_3(\lambda) = \left(I_0(\lambda)\cos\chi \exp - \left[\sec\chi \sum_{k=1}^{K-1} n_k \sum_i \sigma_i(\lambda)R_i(k)\right]\right)$$

The solar zenith angle χ is a function of latitude, day, and time; the absorption coefficients $\sigma_i(\lambda)$ are a function of wavelength; n_K, the column number density of air within the Kth level, is a function of p_*; $I_0(\lambda)$ is the solar flux at the top of the atmosphere; and $R_i(k)$ is the mixing ratio of the ith species at the k level. $J_3(\lambda)$ is the standard expression for converting the flux at the top of the atmosphere to the flux at the top of level K. $J_2(\lambda)$ gives the fraction of that flux which is absorbed in level K. $J_1(\lambda)$ gives the fraction of that absorbed flux which is absorbed by the ith species. The values of $I_0(\lambda)$ used in this calculation were taken from *Ackerman* [1971] and *Simon* [1974].

Since 1976 there have been improved measurements of $K5$, $K6$, and $K7$, as well as the temperature-dependent $O(^1D)$ quantum yield and N_2O photodissociation coefficients. Of particular importance was the measurement of the temperature-dependent N_2O dissociation coefficients [*Selwyn et al.*, 1977] which resulted in a significant reduction in the N_2O destruction rate. *Johnston et al.* [1979] calculated an in-

crease in the N_2O lifetime from 150 to 175 years, while our calculation (not presented here) with 1980 data found 180 years. This change in the calculated atmospheric lifetime of N_2O does not effect the conclusions of this tropospheric study. In a second paper we will discuss the effect of uncertainties in the stratospheric destruction rate on the stratospheric structure of N_2O.

2.3. Source

In the first experiment ('Uniform-Source') we used an initial global surface source of 1.3×10^9 molecules $cm^{-2} s^{-1}$ which was constant in time. This was the basis of our minimum variability experiment. This source strength, when used in a preliminary one-dimensional calculation, resulted in a tropospheric N_2O mixing ratio of 295 ppbv.

For the second experiment ('No-Source') we removed the source, set the N_2O field to the statistically equilibrated distribution generated by the first experiment, integrated for 13 months, and computed the tropospheric distribution and variability. By statistically equilibrated, we mean that the time dependent properties of the distribution are reproducible from one year to the next.

In the third experiment ('Swamp-Source') the global integral of the source strength was not changed from that in the first experiment, and it remained time independent. The source distribution was highly nonuniform, however, with a strength of 2.24×10^{10} molecules $cm^{-2} s^{-1}$ in those surface land boxes which had a model simulated annual rainfall exceeding an arbitrary minimum of 50 inches (127 cm) and a source strength of 0.0 everywhere else. A map of the source distribution is given in Figure 1. This source distribution is not presented as our best estimate of the actual N_2O surface source. Rather, we think of it as a plausable distribution that allows us to evaluate the influence of source spatial variability on the distribution of N_2O and its variability.

2.4. Equilibration

At first glance the 3-D (three-dimensional) simulation of a trace constituent such as N_2O (with a lifetime of order 150 years) appears to be prohibitively difficult. To integrate within 0.1% of the statistically equilibrated value can require as much as 1000 years of model integration. Clearly, more economical means must be used in these types of problems.

Simple 1-D (one-dimensional) model experiments for trace constituents similar to N_2O show that there are two relevant time scales for this problem, the chemical adjustment time scale and the transport adjustment time scale. In the N_2O problem, 1-D 'transport equilibrium' is approached at a faster rate than is 'chemical equilibrium.' This means that, for any initial condition, the basic shape of the 1-D profile is determined much sooner than is the balance between sources and sinks (equilibrium value). In fact, the profile shape can be integrated to acceptable accuracy within about 20 years. Thus, one obvious procedure would be to integrate to 'transport equilibrium' and then adjust the global mean mixing ratio to balance the sources and sinks (or the source to balance the mixing ratio desired).

The above procedure, although effective, is not nearly as efficient or as accurate as other possible procedures. The method to be explained below approaches equilibrium more than 5 times faster than the above approach.

Consider a three-dimensional model atmosphere that has been initialized with a trace constituent distribution that is
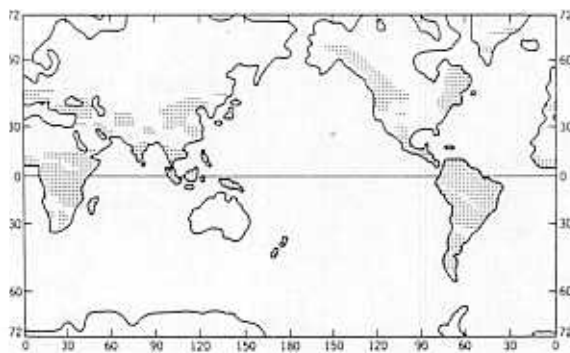

Fig. 1. Dotted areas are source regions for 'Swamp Source' N_2O. They correspond to continental regions over which the model precipitation exceeds 127 cm yr^{-1}.

far from its particular statistical equilibrium. After a period longer than a year, and of the order of the time required for air parcels to exchange meridionally, the annual mean of the horizontal average mixing ratio ($\bar{R}^{H,t}$) begins to exhibit a simpler behavior. This is a regime in which the time rate of change of $\bar{R}^{H,t}$ at a given pressure level begins to diminish smoothly toward a value of zero (the 'apparent equilibrium' solution). This situation can be expressed by using a Taylor series expansion in the form

$$\frac{\partial \bar{R}^{H,t}}{\partial t_{t+\Delta t}} = \frac{\partial \bar{R}^{H,t}}{\partial t_t} + \frac{\partial}{\partial t} \frac{\partial \bar{R}^{H,t}}{\partial t_t} \Delta t +$$

where Δt is the time interval considered. From this expression we can estimate the particular time interval (τ) required to reach apparent equilibrium (when $\partial \bar{R}^{H,t}/\partial t_{t+\tau} \to 0$) at each level as

$$\tau = - \frac{\partial \bar{R}^{H,t}/\partial t_t}{\partial^2 \bar{R}^{H,t}/\partial t_t{}^2} \tag{5}$$

We then use the lowest value of τ so determined ($\tau_{\min}$) to provide a means of reinitializing the R field at a value close to its 'true' equilibrium. This is done at each level by

$$R_{\text{new}} = R_{\text{old}} + \alpha \tau_{\min} \frac{\partial \bar{R}^{H,t}}{\partial t} (p) \tag{6}$$

where α is an empirical coefficient (between 0 and 1) which helps improve the new guess of R. The value we use here is 0.8. Once this reinitialization is made, either the global mean R field or the surface source can be adjusted to put the model into apparent global chemical equilibrium. (For trace constituents in which the chemical time scale is not so long (e.g., ozone), the latter procedure is not required.) Note this is a 1-D correction, although it is applied everywhere in the 3-D model.

The N₂O field has now been set at a 'good guess' for the equilibrium solution. This, however, is only a good approximation. In general, after such a reinitialization, the model will continue to adjust toward its true statistical equilibrium state. Normally, the 3-D model must be integrated for at least 1.5 years before a new reinitialization and a better 'good guess' can be made. We usually find that the adjustment to the field at each successive 'good guess' decreases by a little less than a factor of 10. For example, a +1% correction at one guess would tend to be followed by about a ±0.15% correction at the next guess.

We find that using this procedure allows us to be within about 0.1% of the true equilibrium after 6 years of integration, provided a reasonable guess is used for the initial R field. Otherwise, one extra adjustment would be required to achieve this level of accuracy.

Again, the above procedure corrects the 3-D field in only one dimension, the vertical. This is adequate for the N₂O problem because the mean vertical profile requires the longest time to adjust. In other problems, additional savings could result from a more complicated multidimensional correction. We note that this reinitialization procedure works even better in 1-D and 2-D (two-dimensional) transport models. The simpler structure of such models leads to a simpler and more predictable relaxation toward their final equilibrium states.

3. DESIGN OF EXPERIMENTS

3.1. 'Uniform-Source' N₂O

Since considerable uncertainty existed in 1976 regarding both the size and distribution of tropospheric sources of N₂O, we made the surface source for the first numerical experiment, 'Uniform-Source' N₂O, constant in space and time over the globe. We were then able to determine the importance of large scale motions as a source of mixing ratio variability. By using a zonally symmetric initial field constructed in the manner mentioned in Appendix B, the experiment was integrated for 8 years. Through use of the reinitialization technique of (5) and (6), the model is very near (within 0.15%) to both chemical and transport statistical equilibrium. The experiment demonstrated that a small tropospheric source (17 tg N₂O) is sufficient to produce the temporal relative standard deviation observed in the troposphere and raised the possibility that a relatively small anthropogenic source could have a significant impact on stratospheric N₂O [Levy et al., 1979]. In the next section the results will be discussed in detail.

3.2. 'No-Source' N₂O

In the second experiment, 'No-Source' N₂O, we started with the 'Uniform-Source' N₂O field from year 6 (within 1% of statistical equilibrium) and removed the surface source. This experiment was then integrated for 13 months. The main goal was to determine the influence of the surface source on spatial and temporal variability of tropospheric N₂O. To this end, the surface maps of temporal relative standard deviation and local time series are examined.

3.3. 'Swamp-Source' N₂O

We next wished to examine the effect of source distribution on both tropospheric structure and variability. We would have preferred to run a 'correct' N₂O source experiment, but the spatial distribution of the N₂O source was still not clear in 1978 when this experiment began. While even at this time the picture is not yet clear, the facts do appear to be converging. It was apparent by 1978 that the role of the oceans was becoming much smaller than previously thought, but the variety of potential continental sources and sinks was still quite wide. We chose to use, as our nonuniform source, a land-based source that required high yearly rainfall (127 cm). This experiment, 'Swamp-Source' N₂O, has a highly nonuniform spatial distribution, which is concentrated at low latitudes with a slight excess in the northern hemisphere (N.H.) (see Figure 1). It now appears that the correct N₂O source includes not only wet denitrifying soil regions, but agricultural areas, nitrate-rich fresh water lakes and rivers, and certain regions in the ocean. This N₂O source distribution would, however, still be highly nonuniform. While 'Swamp-Source' N₂O is not expected to duplicate the actual surface distribution, it, together with 'Uniform-Source' N₂O, allows us to examine the range of tropospheric N₂O variability expected for the case of a stratospheric sink balanced by a small surface source.

This integration was started with the 'Uniform-Source' N₂O field from year 6 and was continued until a new statistical equilibrium was reached in the troposphere. As the global source remained constant, no change in the stratosphere was expected nor was any found. In fact, as will

JANUARY "UNIFORM-SOURCE" R_{N_2O} (ppbv)   JULY "UNIFORM-SOURCE" R_{N_2O} (ppbv)

JANUARY "NO-SOURCE" R_{N_2O} (ppbv)   JULY "NO-SOURCE" R_{N_2O} (ppbv)

JANUARY "SWAMP-SOURCE" R_{N_2O} (ppbv)   JULY "SWAMP-SOURCE" R_{N_2O} (ppbv)
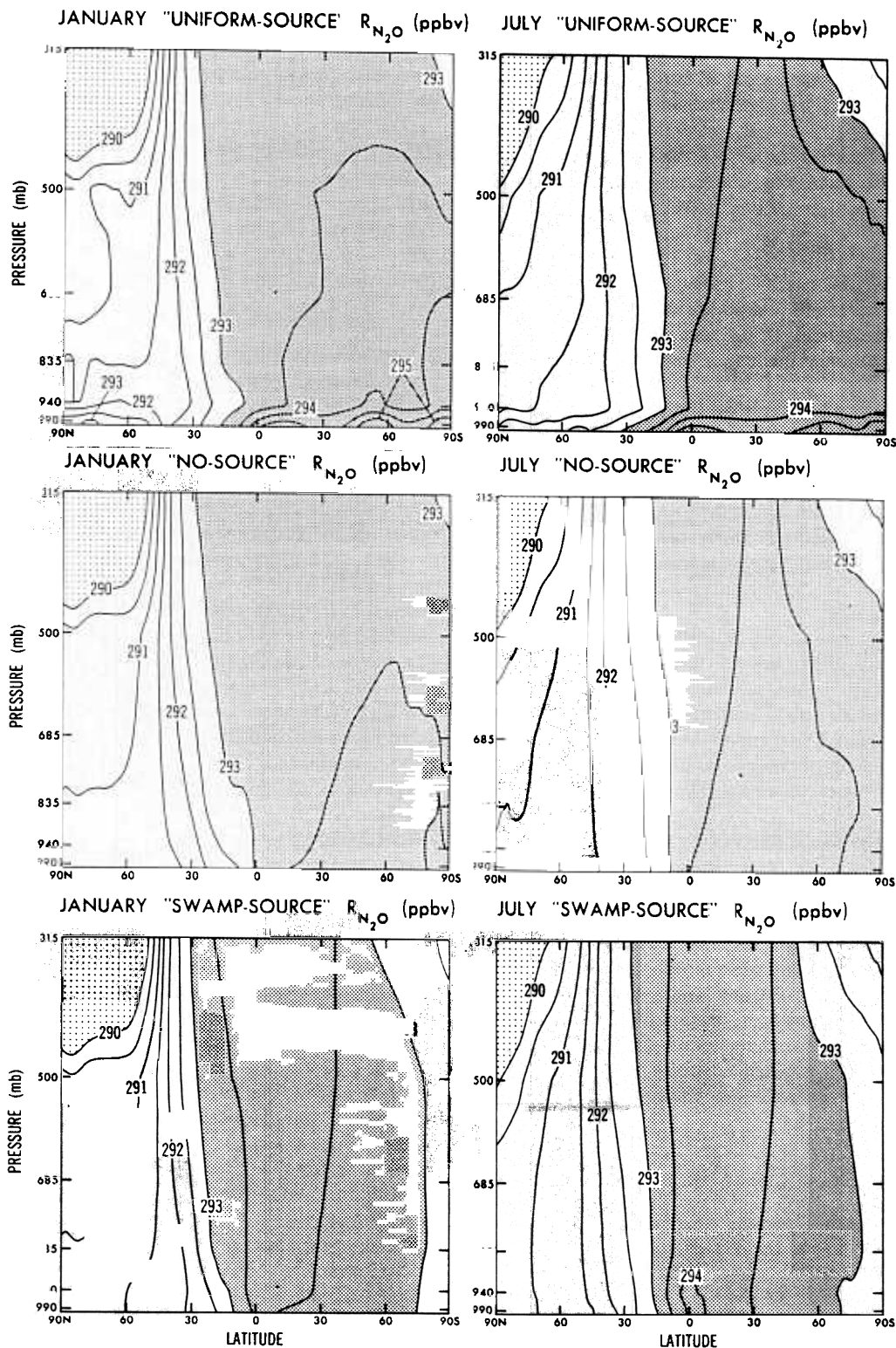
Fig. 2.   Latitude-pressure surface plots of monthly averaged zonal mean N₂O mixing ratios in the troposphere for the three experiments. The contour interval is 0.5 ppbv.

be discussed in the next section, the 500 mbar (~5.5 km) mixing ratio fields for 'Uniform-Source' N₂O and 'Swamp-Source' N₂O are quite similar.

4.   EXPERIMENTAL RESULTS

All the N₂O fields generated by the 'Uniform-Source' and 'Swamp-Source' experiments have a global average surface mixing ratio of 293 ppbv. This value is required to balance the model's three-dimensional transport and stratospheric destruction which produce an atmospheric lifetime of 131 years and the model's arbitrary global source of 17 tg N₂O yr^{-1}. Rather than adjusting the source strength to generate the currently accepted surface mixing ratio (which still ranges between 300 ppbv and 330 ppbv) we kept the original

choice. To compare the model results with measurement data, one need only scale the model data by a constant factor that brings the globally averaged surface mixing ratios into agreement. Most of the significant tropospheric results reported in this paper deal with variability, for which the exact surface value mixing ratio is irrelevant. In fact, recent measurements appear to be converging to ~300 ppbv [*Weiss and Craig*, 1976; *Connell et al.*, 1980; *Goldan et al.*, 1981].

4.1 Zonal Mean Fields

First, we will discuss N$_2$O mixing ratios which have been averaged over a month's time and around a latitude circle. These zonal mean fields ($\bar{R}^\lambda_{N_2O}$) are presented in Figure 2 for all three source experiments as July and January monthly averages.

The first point to observe is that the upper tropospheric fields are very similar in all three experiments and therefore nearly independent of the source distribution. At 500 mbar in the middle troposphere, the surface source distribution has very little effect on the tropospheric mixing ratio. In the bulk of the southern hemisphere (S.H.) troposphere, $\bar{R}^\lambda_{N_2O}$ is well mixed vertically while there is a small gradient in the north. This feature is not significantly influenced by season or source distribution.

Only in the lowest two model layers does the source distribution have much impact. 'Uniform-Source' N$_2$O with a hemispherically balanced source has ~1% excess in the S.H., with a minimum at northern high latitudes. This is a result of the model's relatively more effective downward transport of lower stratospheric air in the northern hemisphere which dilutes the tropospheric air with low N$_2$O air from the stratosphere. This feature of the model has been demonstrated previously in our stratospheric ozone experiment [*Mahlman et al.*, 1980]. The small vertical gradient for N$_2$O keeps the interhemispheric asymmetry down at the 1% level. Turning off the source does not appreciably change the latitudinal structure. The 'Swamp-Source' N$_2$O experiment does not have enough excess production in the N.H. to combat the increased dilution and reverse the latitudinal gradient. It does, however, produce a maximum in the equatorial region where the source is strongest.

We will now consider a measure of tracer variability, the longitudinal relative standard deviation

$$V_\lambda = 100 \left[\sum_{n=1}^{N} \frac{(R_n - \bar{R}^\lambda)^2}{N} \right]^{1/2} \bigg/ \bar{R}^\lambda \qquad (7)$$

V_λ is calculated relative to the zonal mean, $\bar{R}^\lambda$. The summation over n is taken around a given latitude circle for N points. Time-averaged latitude-pressure distributions for January and July ($\bar{V}_\lambda$) are given in Figure 3.

As should be expected, given the similarity in the monthly mean $\bar{R}^\lambda_{N_2O}$ fields down to 500 mbar for the three source experiments, the $\bar{V}_\lambda$ fields are also very similar at 500 mbar. As reported earlier [*Levy et al.*, 1979], the maxima in $\bar{V}_\lambda$ occur in regions of maximum mixing ratio gradient. This location is consistent with our earlier expectation that the large-scale motions operating on mixing ratio gradients would produce the variability. Figure 3 shows the influence of the surface source on variability in the lower troposphere. 'Uniform-Source' N$_2$O has a minimum in $\bar{V}_\lambda$ stretching from the equator to 60°S and a maximum in the wintertime high latitudes (above 60°) of both hemispheres.

The 'No-Source' N$_2$O distribution has a uniformly low $\bar{V}_\lambda$,

with the exception of a small winter increase in northern middle and high latitudes due to the active downward transport in that region at that time. The 'Swamp-Source' N$_2$O distribution has a higher $\bar{V}_\lambda$ in general and a maximum, rather than a minimum, in the equatorial boundary layer. This is a result of the much stronger local source and its nonuniform spatial distribution. The dependence of spatial and temporal variability in the boundary layer on source strength and distribution will be examined in more detail in the following sections that consider both latitude-longitude fields and local time series.

4.2 Horizontal Fields

While longitudinal mean cross sections do show large-scale latitudinal features, they are not particularly useful for comparisons with the type of atmospheric data normally gathered unless the fields under consideration are close to zonally symmetric. As will be shown in this section, there is considerable longitudinal asymmetry in the mixing ratio and variability fields generated by the three experiments, particularly in the boundary layer.

4.2.1. Middle troposphere fields.
The 500 mbar monthly mean N$_2$O mixing ratio fields ($\bar{R}'_{N_2O}$) for January and July are given in Figure 4. Only the 'Swamp-Source' N$_2$O data is shown because the other fields are almost the same, except for the small maximums located over strong source regions in Brazil and southern Africa. In general, the time-mean fields are almost zonally symmetric with a uniform distribution in the S.H. and a slight latitudinal gradient in the N.H. with a minimum at high latitudes. This feature is controlled by the model's dynamics and should be insensitive to the surface source distribution. A comparison with measurements would be very informative. Currently, the only available data is not of a high enough precision to confirm or deny the existence of the small gradient (H. E. Heidt, private communication, 1981). The most significant asymmetric feature is the 291 ppbv contour line which represents the $\bar{R}'_{N_2O}$ minimum. In January, due to more downward transport of low N$_2$O air from the lower stratosphere, it has pushed quite far south over eastern Siberia, the north Pacific, and North America. In July the 291 ppbv contour recedes northward. In general the 500 mbar $\bar{R}'_{N_2O}$ fields, with the exception of northern high latitudes, are zonally symmetric and independent of season. They are not significantly influenced, excluding the two small local source regions in Brazil and southern Africa, by the surface source distribution and local strength. A combination of strong local sources and tropical convection is responsible for those local 500 mbar maximums.

The monthly mean 500 mbar fields of temporal relative standard deviation, V_t, are also given in Figure 4 for January and July.

$$V_t = 100 \left[\sum_{i=1}^{N} \frac{(R_i - \bar{R}')^2}{N} \right]^{1/2} \bigg/ \bar{R}' \qquad (8)$$

where $\bar{R}'$ is the monthly mean mixing ratio for a given box and i is summed over the number of days in the month N. The R_i are taken once each model day. There is some error in V_t due to sampling only once each day. A check of 20 points over the globe, using complete model data, found that, with one-a-day sampling, monthly V_t decreased less than 10% in the boundary layer and generally less than 10% at 500 mbar. In regions where V_t is comparatively low, the
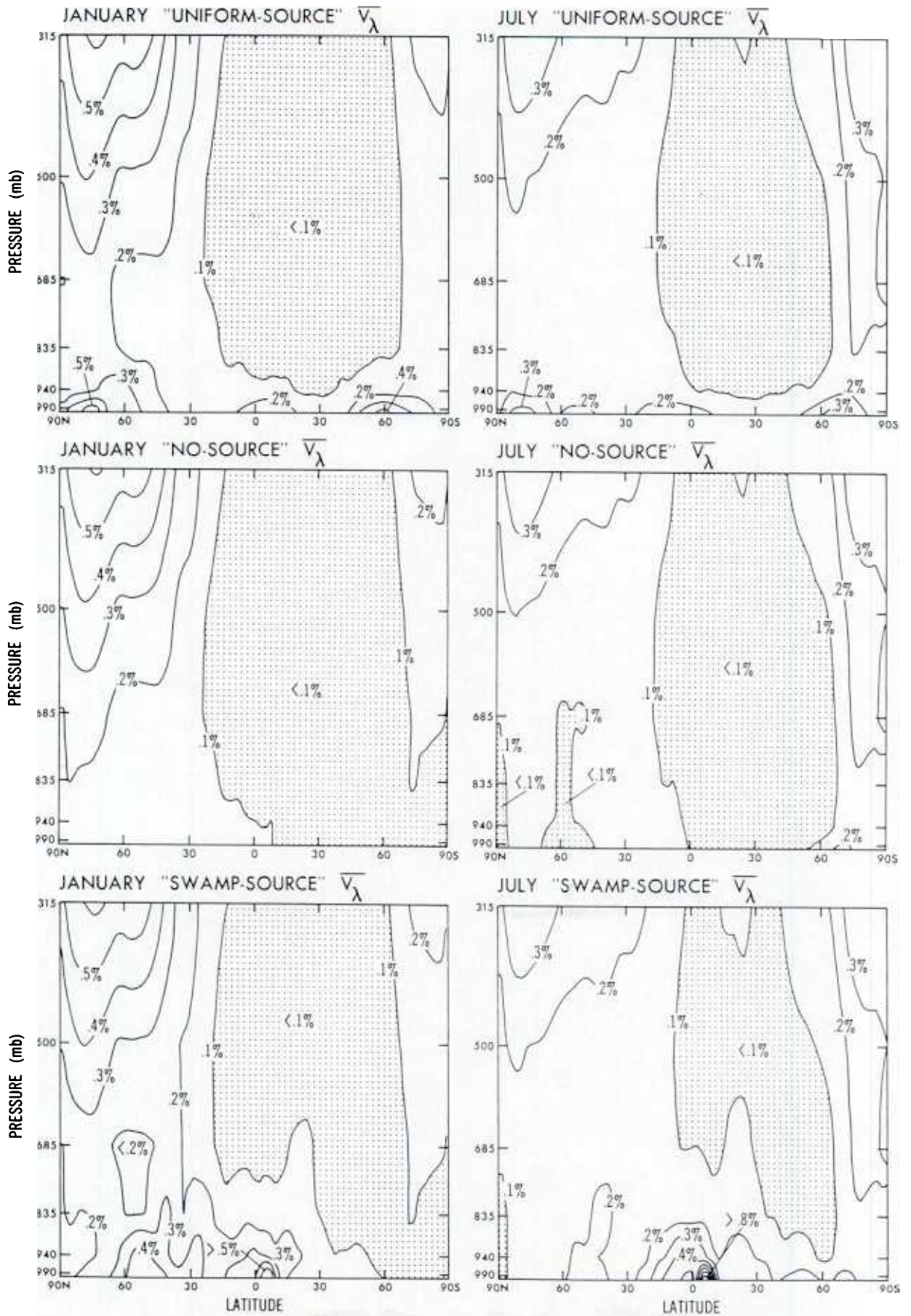
Fig. 3. Latitude-pressure plots of the monthly mean longitudinal relative standard deviation ($\overline{V}_\lambda$) for the three experiments. The contour interval is 0.1%.
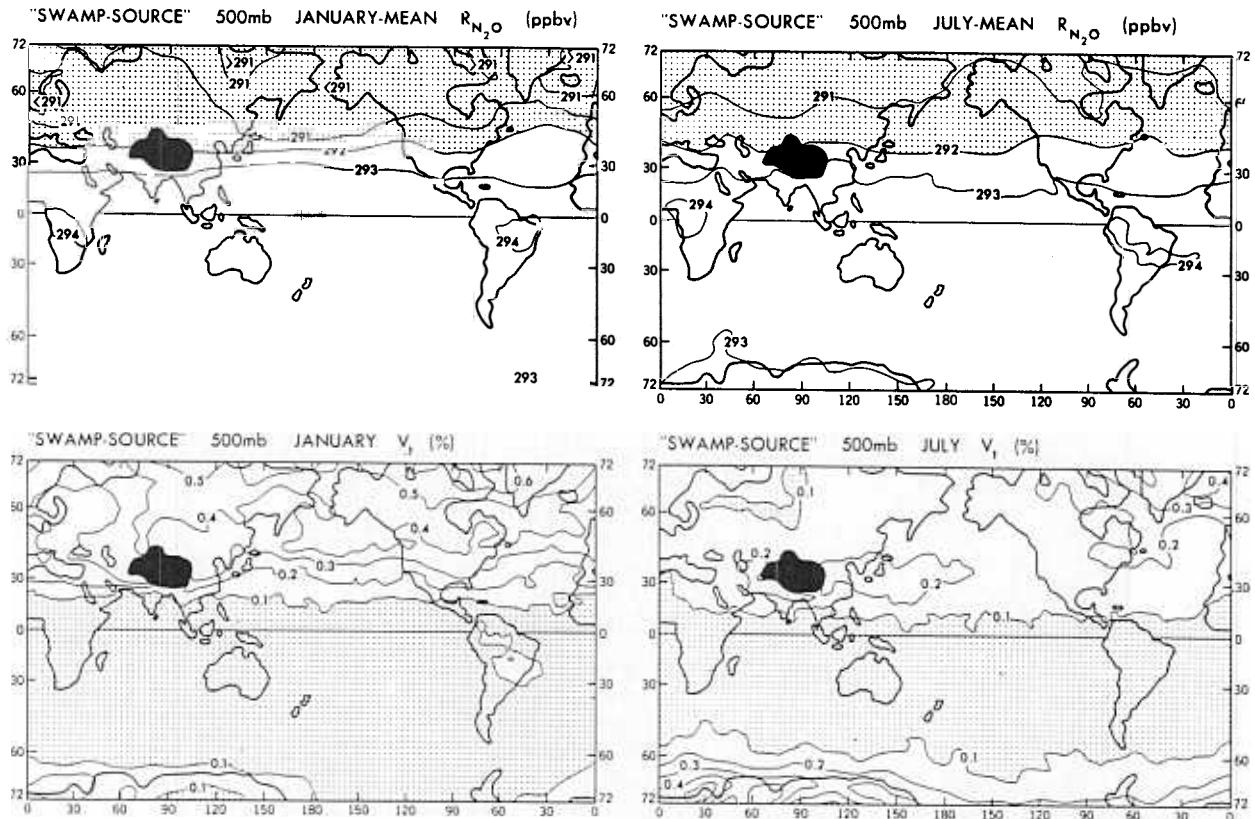
Fig. 4. January and July maps of R_{N_2O} and V_t at 500 mbar. The solid black area shows where the Himalayan Plateau intersects the 500 mbar surface. The contour interval for R_{N_2O} is 1.0 ppbv, and the contour interval for V_t is 0.1%.

one-a-day sampling led to reductions as high as 20%. The dominant fluctuations are on synoptic time scales (3–7 days) and thus are well captured by sampling once each day.

Just as for $\bar{R}'_{N_2O}$, the monthly V_t fields at 500 mbar are hardly influenced by the source distribution. Therefore, only the 'Uniform-Source' V_t fields are shown. The tropics and most of the S.H. have $V_t < 0.1\%$. There is a large wintertime maximum exceeding 0.4% in the northern middle- and high-latitudes, which shows up in the same region that was bounded by the 291 ppbv contour. This minimum in N₂O and maximum in V_t is the result of the strong downward transport of stratospheric air associated with the jet stream off Japan in the upper troposphere [Mahlman et al., 1980], and the fact that these latitudes are the region of maximum model transient cyclone disturbances during January [Mahlman and Moxim, 1978]. A high latitude maximum in variability, $V_t > 0.4\%$, shows up over a smaller area in the S.H. winter.

As previously mentioned, the 500 mbar V_t fields are very similar for all three experiments. Local variability in the middle troposphere is essentially independent of the surface source distribution. The model's middle troposphere V_t's range from 0.1 to 0.5%, and are a result of the transient large scale motions acting on both vertical and horizontal gradients of mixing ratio.

4.2.2. *Boundary layer fields*.   In the boundary layer we can observe the impact of the surface source distribution and strength on both spatial and temporal variability. The January and July monthly mean surface N₂O fields for 'Uniform-Source' N₂O and 'Swamp-Source' N₂O are given in Figure 5.

While the 'Uniform-Source' N₂O surface fields retain some of the general features seen in the zonal mean fields of Figure 3, a great deal of longitudinal structure is present. In the equatorial region a mixing ratio maximum forms just south of the model's intertropical convergence zone (ITCZ). (See Figures 2 and 4 in Levy et al. [1980] for July and January mean surface streamlines.) The equatorward movement of air south of the ITCZ results in an accumulation of N₂O in the boundary layer. If there is no transport out of the bottom model layer, N₂O will accumulate at the rate of 0.3 ppbv day⁻¹ in the 'Uniform-Source' experiment. The time required to build up the excess south of the ITCZ is consistent with the time required for an air parcel to move from the subtropical anticyclones to the ITCZ. In the summer S.H. the continents are uniformly low in N₂O. This is due to the much higher convective activity over land which preferentially mixes the continental boundary layer. In the N. H. there is, in general, a decrease in N₂O at higher latitudes. However, the gradient is far from zonally symmetric, showing considerable variation between land and ocean.

The most obvious feature of the 'Swamp-Source' N₂O boundary layer is the concentration of $\bar{R}'_{N_2O}$ in the source regions. In the absence of vertical transport, N₂O accumulates in the lowest model level at a rate of 4.6 ppbv day⁻¹ in those areas with a source. Accumulations in excess of 5% over background (310 ppbv versus 295 ppbv) are common in the model source region and require build-up times of less than 4 days. Over North America we see maximum accumulation in the northeast during the winter and in the northwest during the summer. The increase in N₂O accumulation during the winter in the northeast is the result of decreased convective mixing out of the boundary layer during winter.
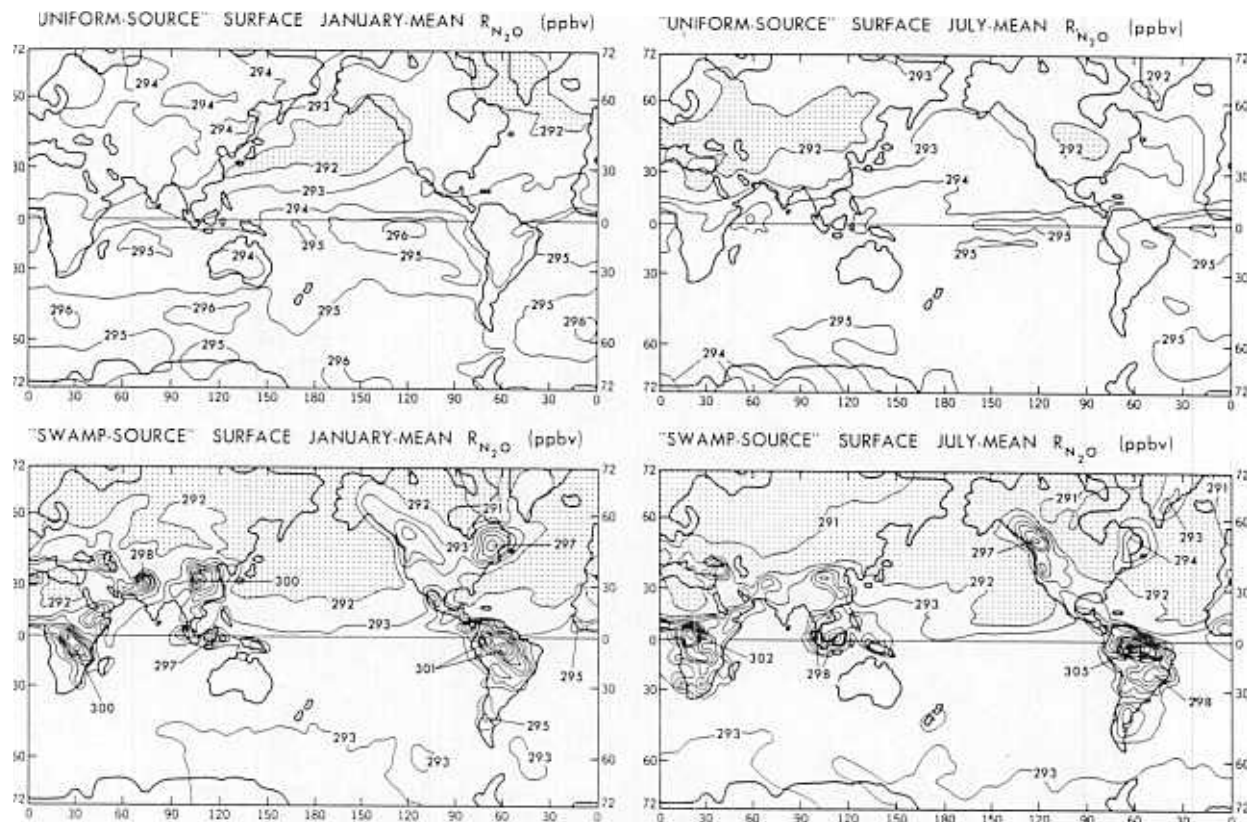
Fig. 5. January and July maps of monthly mean N₂O mixing ratio at 80 m above the surface for 'Uniform-Source' and 'Swamp-Source' experiments. The contour interval is 1.0 ppbv. Dotted areas have $R_{N_2O} \leq 292$ ppbv.

In the northwest, the model's summertime decrease in the on-shore flow of relatively dilute maritime air [see Figures 2 and 4 in *Levy et al.*, 1980] results in a summertime maximum of N₂O. Maximum accumulation over the tropics and the southern subtropics occurs in July. In the S. H. oceanic boundary layer (which has no surface source) 'Swamp-Source' N₂O has a very uniform field. In the N.H. non-source regions, $\bar{R}'_{N_2O}$ is much less uniform due to dilution by large-scale vertical transport. From these two experiments we see that nonuniform local sources should lead to significant excess N₂O in the source region of the boundary layer relative to the global mean; that the distribution of N₂O over the oceans is significantly influenced by the presence or absence of a surface source; and that the N₂O distributions over the northern mid-latitude continents are influenced by the large-scale tropospheric motions.

By examining the V_t fields for all three source experiments (see Figure 6), we gain further insight into the influence of source strength and distribution on N₂O in the boundary layer. In general, just as was observed in Figure 3, regions of high variability are located near those areas that have strong vertical or horizontal mixing ratio gradients.

To examine seasonal effects, we consider the January and July mean V_t fields for the 'Uniform-Source' experiment. We find January $V_t > 0.4\%$ over most of the continental N.H. north of 30°N with the exception of western Europe and the western United States. The southern Pacific south of 40°S which had high N₂O also has $V_t > 0.5\%$. The one other region of high V_t is the region just south of the ITCZ where there was significant N₂O accumulation. The S.H. continents which have deep summertime convective mixing also

have low variability, $V_t < 0.1\%$. In July all the large values disappear, except for the southern high latitudes. A maximum does form northeast of Japan as a result of strong cyclonic activity in the model northern Pacific. There is also the remains of a weak maximum in the region of the ITCZ. The January maxima in Europe and the United States are replaced with minimums. It is clear that the interaction of a uniform source and the atmospheric wind fields results in a highly nonuniform V_t field.

For the case with the surface source removed ('No-Source' N₂O), we find a much more uniform V_t field. In January the southern hemisphere V_t drops to $< 0.1\%$, and the only regions in the northern hemisphere with $V_t > 0.2\%$ are over the Himalayan Plateau, Canada, and the central Atlantic. In July, with the exception of high variability over Antarctica and a region over the central Pacific with $V_t > 0.2\%$, the rest of the boundary layer has $V_t < 0.1\%$. These low values indicate that much of the variability in the surface layer results from the presence of a surface source, even when the source is small and uniformly distributed. The exception to this would be the wintertime middle and high latitude regions which derive a fraction of their boundary layer variability from sporadic downward transport of lower stratosphere air containing lower N₂O mixing ratios.

The V_t fields from 'Swamp-Source' are quite interesting. The regions of high variability are located over and near the regions of high N₂O, which in turn are located over sources. It is common to find $V_t > 2\%$ in these regions. On the other hand most of the southern hemispheric ocean boundary layer (where there is no source) has $V_t < 0.1\%$ as does summertime USSR. Ignoring the wintertime high latitudes,

"UNIFORM-SOURCE" SURFACE JANUARY V_t (%)   "UNIFORM-SOURCE" SURFACE JULY V_t (%)

"NO-SOURCE" SURFACE JANUARY V_t (%)   "NO-SOURCE" SURFACE JULY V_t (%)

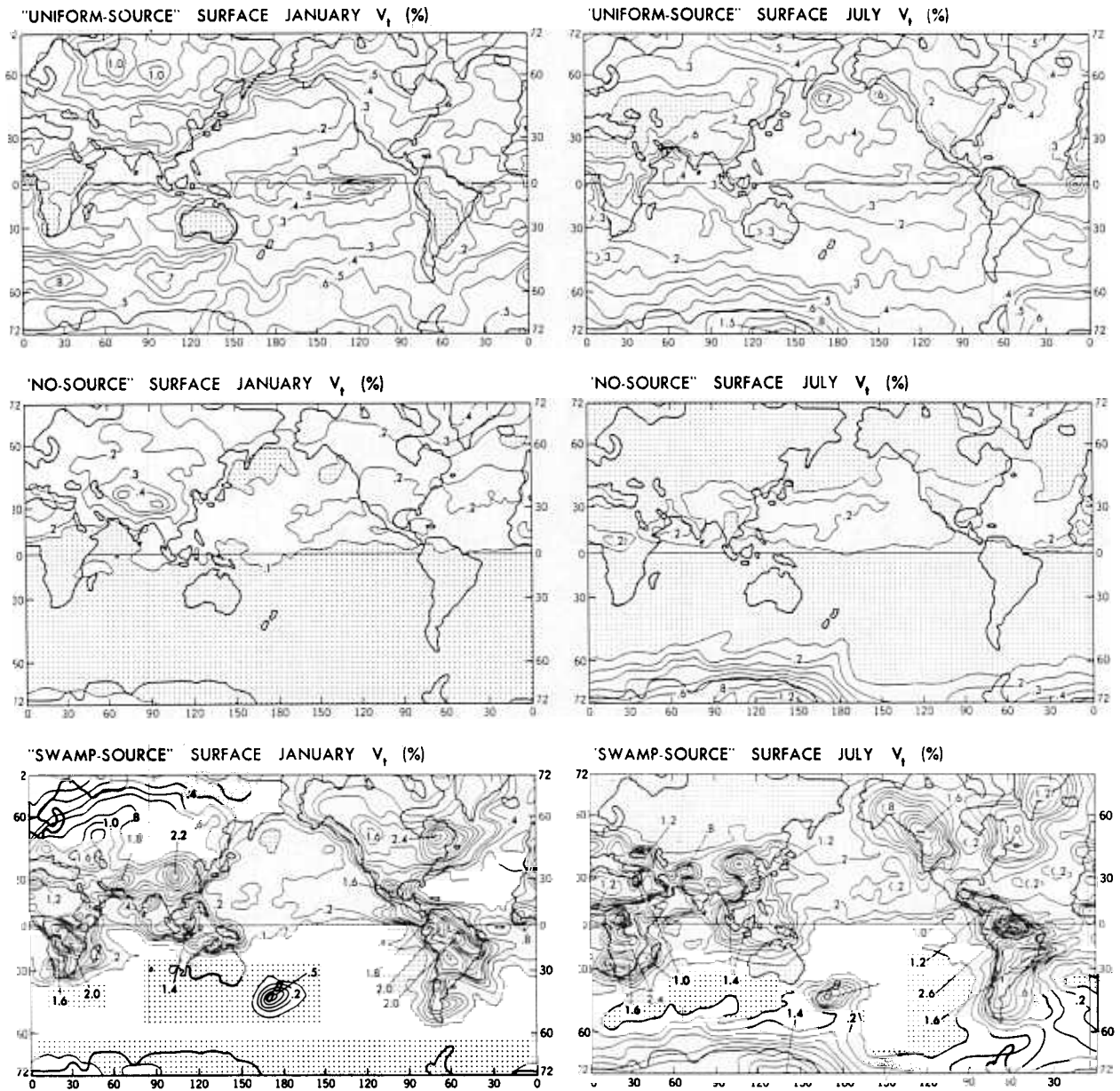"SWAMP-SOURCE" SURFACE JANUARY V_t (%)   "SWAMP-SOURCE" SURFACE JULY V_t (%)

Fig. 6. January and July maps of the temporal relative standard deviation at 80 m above the surface for all three experiments. The contour interval is 0.1% with the exception of the 'Swamp-Source' maps where it increases to 0.2% above 0.6%. Dotted areas have $V_t \leq 0.1\%$.

we would have a qualitative representation of the 'Swamp-Source' V_t fields by superimposing the source field for 'Swamp-Source' (Figure 1) on the 'No-Source' V_t fields.

In general, we can conclude that, where there is no nearby surface source, there will be very low variability in the boundary layer ($V_t \gtrsim 0.1\%$), and that near the source regions V_t will be influenced by both the local source strength and the local meteorology. Since it now appears that the actual N_2O sources are far from uniform, it is evident that measurements of N_2O and its variability should be an important tool for determining the presence of a source. Calculations of V_t in regions assumed to be far from sources will not tell much about the source structure, other than confirming that the measurements are far from a source. It is also clear, given the wide range of V_t values possible for even the most spatially uniform of sources, that the application of Junge's

empirical relationship [Junge, 1974] relating temporal relative standard deviation to atmospheric lifetime is not appropriate for boundary layer measurements. There may, however, be a relationship between V_t in the middle troposphere and the atmospheric lifetime of N_2O through the dependence of V_t on the vertical gradient in the stratosphere, which itself depends on the atmospheric lifetime.

4.2.3. Comparison with measurements. Weiss [1981] has recently reported an extensive series of N_2O measurements made in the atmospheric boundary layer. Most of the data was gathered on sea voyages, though values from Antarctica, Hawaii, and Alaska were also included. While the relative standard deviation for his data (0.2%) is consistent with our model predictions for nonsource regions, he also finds a slight north-south N_2O gradient with a small excess (~0.8 ppbv) in the northern hemisphere. This is

opposite to the results of our idealized source calculations. If our model's transport asymmetry is correct, it would appear that the true sources release much more N_2O into the northern hemisphere. The distribution of N_2O in the boundary layer is quite sensitive to the source structure in the model. However, the middle and upper troposphere N_2O distribution, with a minimum in the northern hemisphere, is controlled by transport from the lower stratosphere and is only weakly influenced by the boundary layer source distribution. Based on the model results, we would conclude that the measured N_2O distribution in the boundary layer may be quite different from the distribution in the troposphere as a whole. We plan to explore this possibility in a future experiment. It should also be noted that a series of measurements by *Singh et al.* [1979], with a relative standard deviation of 0.8%, found no meridional gradient in the atmospheric boundary layer over the Pacific.

4.3 Local Time Series

It is not likely in the near future that sufficient N_2O data will exist to make meaningful quantitative comparisons with either the zonal mean fields in Figures 2 and 3 or the $\bar{R}'_{N_2O}$ and V_t surface fields in Figures 4, 5, and 6. There is, however, considerable information to be gained from local time series. While global properties such as atmospheric lifetime are beyond the reach of local measurements, the time series will provide information about local sources and sinks. A small network [*Cunnold et al.*, 1978] has been established to make such measurements and some preliminary measurements from the state of Washington have been reported [*Pierotti and Rasmussen*, 1977; *Pierotti et al.*, 1978]. Since we find that boundary layer N_2O is most responsive to source strength and distribution, and that time series measurements in that region will be available in the future, we concentrate there. It should be made clear that the model time series represents an average over a box of approximately 265 km on a side. Furthermore, the individual box is not isolated from its neighbors. A particular model time series is representative of a set of boxes, not a specific location. The latitude and longitude are merely given to identify the region in the model from which the data is taken.

Before examining individual series in detail, we should consider the proper treatment of both the model and measurement data. We choose to smooth the data by taking a 24-hour running mean. This procedure will greatly reduce high frequency fluctuations. A comparison of the complete data set and the smoothed set for the surface box containing Tallahassee, Florida (30°N, 84°W) from the 'Uniform-Source' experiment is given in Figure 7. Examining the time series and its spectrum for every time step, 56 data points per day (Figure 7a), we find a sharp drop off for periods less than 3 days and a dominance of power in the synoptic range of 3–10 days. An alternative, though qualitative, estimate of the dominant periods of fluctuation can be made by counting the days between the peaks. There is also a significant one year cycle, due to the spring minimum and fall maximum, as discussed previously [*Levy et al.*, 1979].

One must remember that atmospheric phenomena, while frequently wave-like, are not a simple combination of waves with different periods. Rather, the atmosphere is a complex mixture of random, stochastic, and wave-like processes which presents a confusing signal. Analysis techniques such as autocorrelations, structure functions, and frequency spec-

tra do not, generally, provide simple results that lead to straightforward conclusions. In this particular case we did find that frequency spectra were of some use, though not enought to justify the presentation of a separate spectrum for each time series.

We have provided an example of these spectra in Figure 7. There is the same general shape for the other time series, a slow drop in amplitude from the 1 year period down to the 3 day period followed by a much sharper drop in amplitude for shorter periods. The time series with obvious seasonal structure (Tallahasee and Ann Arbor) show relatively large amplitudes for the 1 year period, while the Panama time series has a maximum amplitude for the periods of 3–30 days. Plots of autocorrelation coefficients and structure functions contain no added information and, therefore, are not shown. A visual examination of the 24 hour running mean time series (Figure 7b) shows no significant difference between it and the one in Figure 7a. The more detailed spectral analysis shows no significant change in amplitude for periods longer than 3 days. There is a sharp drop off in the amplitude for periods <1 day, and the deep minimum at the 24 hour period confirms the theoretical conclusion that the 24 hour running mean should cancel this period exactly [e.g., *Holloway*, 1958]. The relative standard deviation is only reduced 2.5% by this smoothing. It is clear that the model data is only weakly contaminated by high frequency fluctuations.

We have two concerns regarding future comparisons between model and measured time series. The first is that the measured data might be dominated by high frequency fluctuations. While these can be due to both real phenomena and random measurement error, they must be removed from the data to provide a realistic comparison with the model data, which can only be expected to resolve fluctuations with a period of 1 day or more. If there is a large high frequency component in the experimental data, a spectral analysis should determine whether it is essentially white noise (i.e., experimental error) or whether the power is in a few periods that represent either real physical processes or systematic errors. Our second concern is that the limited time resolution and the 1 day averaging of the measurements can alias spurious and real high-frequency fluctuations into the lower-frequency, synoptic scale, fluctuations. It is important for those performing the measurements to prove that their measurement frequency is sufficient to capture the dominant fluctuations in the data and to insure that random fluctuations due to experimental error are not allowed to overwhelm legitimate lower frequency fluctuations. This precaution might require sampling more frequently than normally planned for a given averaging period. Thus, it must be determined that either there is no large high-frequency signal, or, if one exists, that the proposed sampling interval and 1 day averaging does not result in significant aliasing into lower frequencies. If there is a strong high-frequency signal (period <1 day), it would be important to determine its nature and source.

The model time series for two representative polar grid boxes that contain Pt. Barrow (71°N, 157°W) in the N.H. and Byrd Station (80°S, 120°W) in the S.H. are shown in Figure 8. All the time series data consists of 56 points per day which have been smoothed by plotting the 24 hour running mean rather than the individual points. The two 'Uniform-Source' N_2O time series for the high latitude points show no particu-
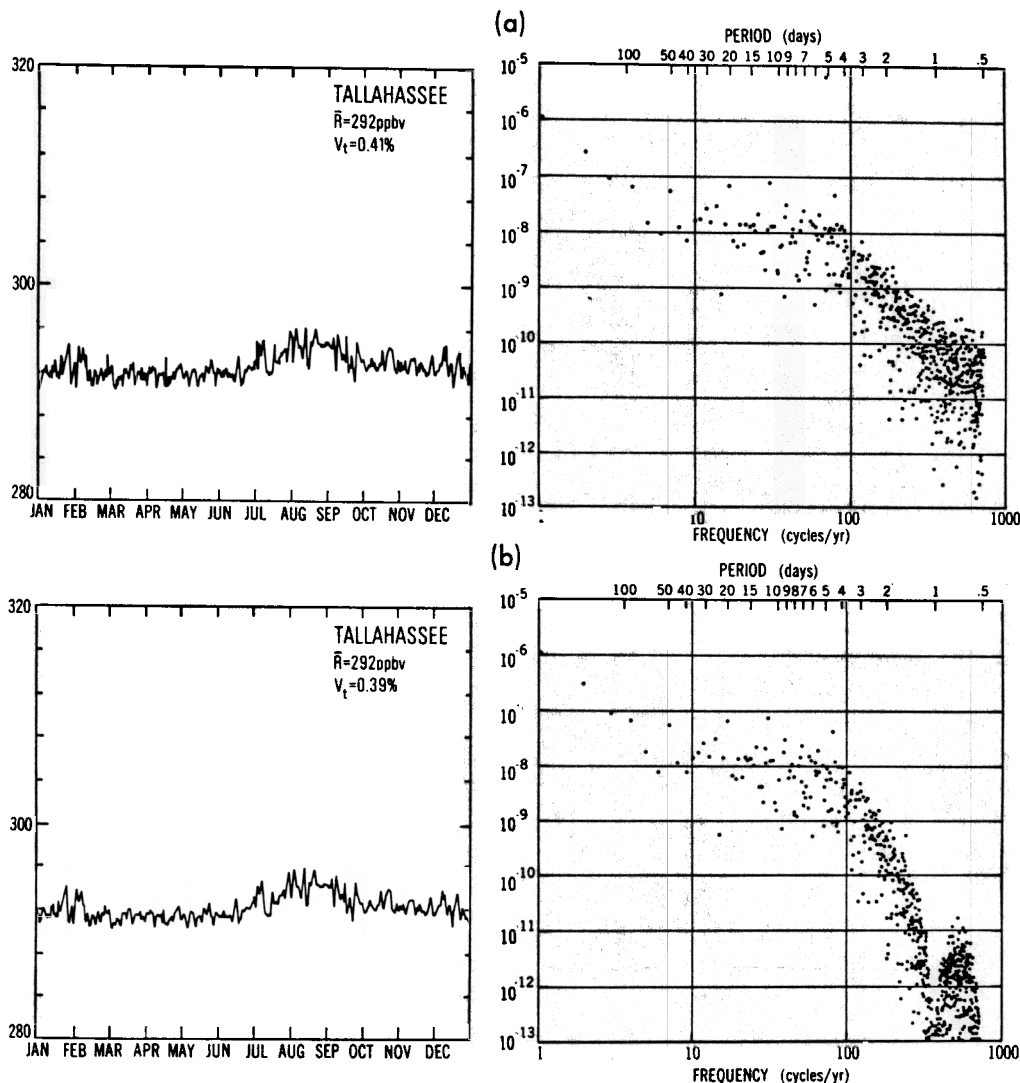
Fig. 7. Time series (ppbv) and frequency spectra (ppbv^2 cycles^{-1} yr) for 1 year of model mixing ratio data from a surface box containing Tallahassee, Florida (30°N, 84°W). In Figure 7a. all 56 data points/day were used without any smoothing, while in Figure 7b a 24 hour running average was applied to the same data. Yearly V_t is calculated with the yearly mean R_{N_2O}.

lar seasonal structure, but do have a relatively high variability which ranges from 0.5 to 1.0%. The 'No-Source' N$_2$O series, having no boundary layer accumulation, reveal the contribution of wintertime downward transport to variability in the boundary layer. The level of variability resulting from the action of transient large-scale motions on mixing ratio gradients produces wintertime maximum $V_t \sim 0.25\%$ and summertime minimums of $V_t < 0.1\%$. For 'Swamp-Source' N$_2$O, we see that the time series structure for Byrd Station in Antarctica, far from any source, is virtually identical to the 'No-Source' N$_2$O series. The 'Swamp-Source' N$_2$O time series for Point Barrow, while retaining the seasonal structure revealed by 'No-Source' N$_2$O, is near a relatively large source region (see Figure 1). The range of monthly V_t values (0.5–0.2%) is greater than for 'No-Source,' but still significantly less than that found for 'Uniform-Source' which had a small uniform source throughout the polar region. The main features of the time series in the polar region boundary layer are a strong seasonal cycle with a wintertime maximum in variability and a strong sensitivity to source strength and location. Both the northern and southern polar regions are

subject to frequent 5–10 day periods of boundary layer accumulation which, given a constant local source as in 'Uniform-Source' N$_2$O, produce regional gradients in N$_2$O that are a source of local variability. Without the source, this is not observed.

In Figure 9 we consider time series for mid-latitude points in both hemispheres. Ann Arbor (42°N, 85°W) shows strong seasonal structure, due to the strong wintertime downward transport of low N$_2$O air. In this case the seasonal structure dominates any nonseasonal source related effects, though the presence of this source does enhance the high wintertime variability. Summertime V_t's are quite low ranging from 0.1% for 'No-Source' N$_2$O to 0.2% for 'Swamp-Source' N$_2$O. Over the continental mid-latitudes of the S.H., we have the same seasonal behavior, but a different driving mechanism. The enhanced summertime convection over the land leads to a well-mixed local troposphere which, because of the lack of a vertical gradient, results in V_t minimums of 0.1% regardless of source structure. In the wintertime, although there is no strong model downward transport at Capetown (34°S, 19°E), the combination of a surface source
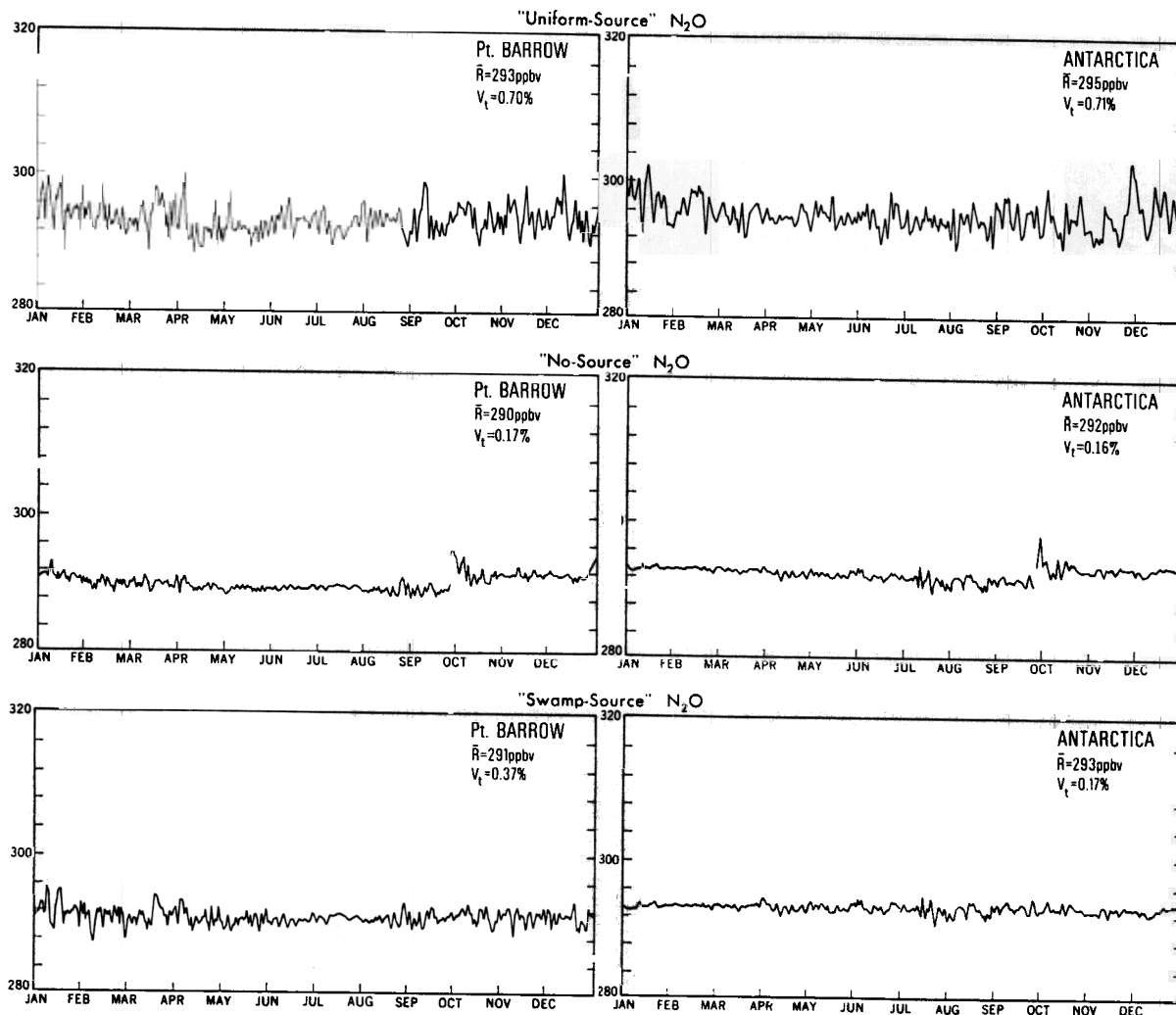
SIMULATED LOCAL SURFACE TIME SERIES

Fig. 8. One year time series of model N_2O mixing ratio (ppbv) for two high-latitude surface boxes. Pt. Barrow (71°N, 157°W) and Antarctica (80°S, 120°W), for all three experiments. Yearly V_t for the 'Uniform-Source' and 'Swamp-Source' experiments is calculated with the yearly mean N_2O mixing ratio and averaged over a year. For the 'No-Source' experiments, V_t is the average of the 12 monthly V_t's. This is done to greatly reduce the contribution of the artificial trend in N_2O which results from the lack of a source. This same artificial trend results in a discontinuity in the time series at October, the starting point for the experiment.

and the seasonal tropospheric wind fields produce monthly V_t's ranging from 0.3% for 'Uniform-Source' N_2O to 0.7% for 'Swamp-Source' N_2O. The lack of any significant variability for 'No-Source' N_2O ($V_t < 0.1\%$ throughout the year) demonstrates that, unlike Ann Arbor, boundary layer accumulation is the dominant source of variability.

In Figure 10 we consider a grid box on the coast of Washington which has a very different model meteorology from midcontinent regions. There is a strong onshore flow in the winter with occasional interruptions and much weaker flow in the summer. It also has a different seasonal structure in monthly V_t, with a maximum in the summer and a minimum in the winter. This is weakly present in 'Uniform-Source' N_2O with a range of 0.35–0.20% and quite strong (1.0–0.5%) in 'Swamp-Source' N_2O. This seasonal behavior is the reverse of that found at the Ann Arbor box and its amplitude depends on source strength. A comparison of these series with data measured by *Pierotti et al.* [1978]

suggests that, in the real atmosphere, western Washington is not near a strong N_2O source region.

In Figure 11 we examine time series for two tropical points, Panama (9°N, 80°W) and Samoa (14°S, 171°W), which have very interesting responses in the 'Swamp-Source' experiment. First, we note that there are no significant seasonal features in the Samoa series from 'Uniform-Source' and that yearly $V_t = 0.35\%$ ($\bar{R}'$ in (8) is the year mean), an average value for the troposphere. For the Panama series, the first half of the year has the monthly V_t's ranging from 0.1 to 0.2%, while in the second half they range from 0.25 to 0.35%. When the surface source is turned off, monthly V_t's drop to a steady low value for both, 0.17–0.08% for Panama and 0.10–0.05% for Samoa. With 'Swamp-Source' we have one site, Panama, that is in the midst of a large source region and one, Samoa, that is in a large nonsource region (see Figure 1). The results demonstrate the impact of a local source on surface variability. The

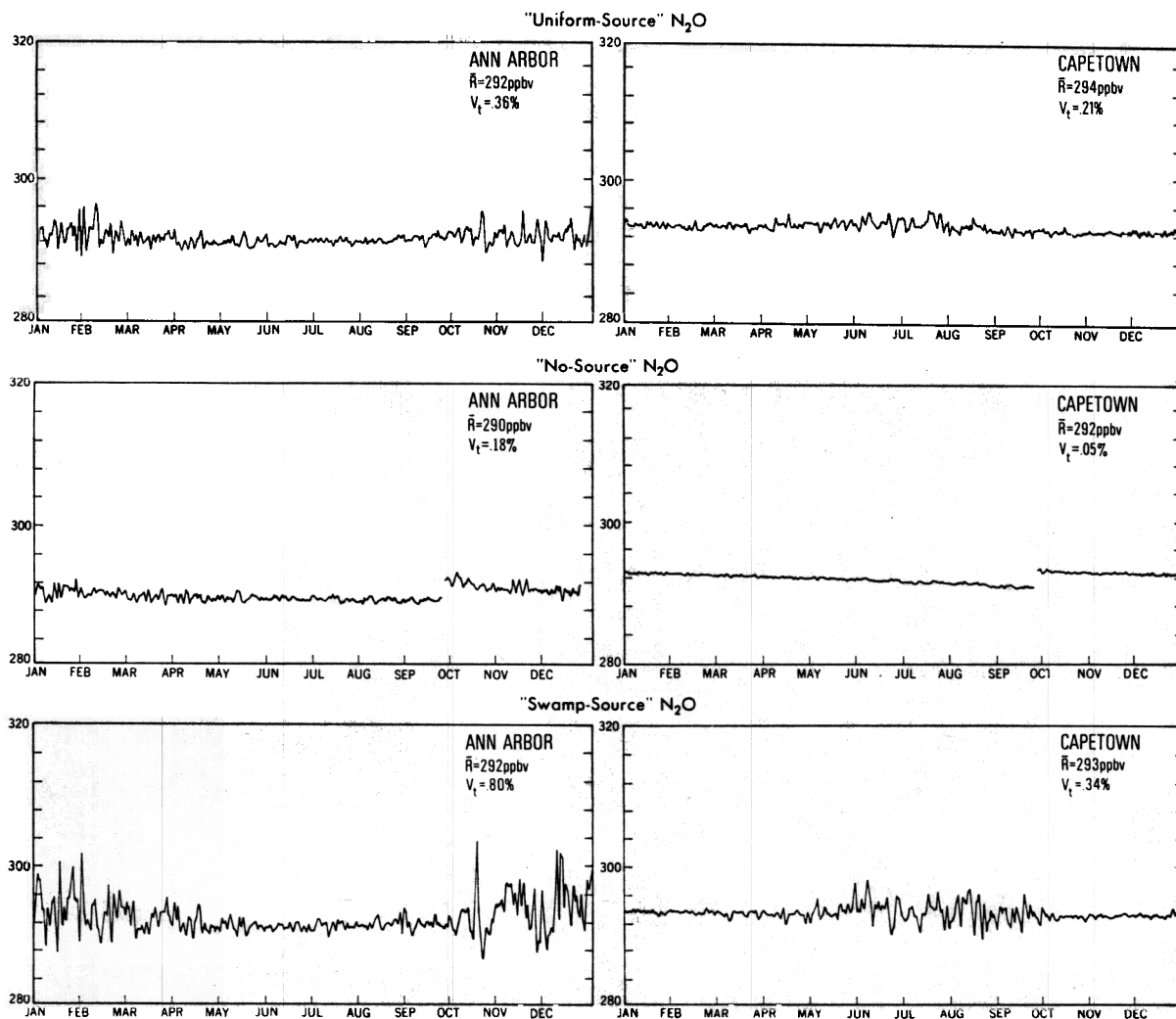SIMULATED LOCAL SURFACE TIME SERIES

Fig. 9. One year time series (ppbv) for two mid-latitude surface boxes, Ann Arbor (42°N, 85°W) and Capetown (34°S, 19°E), for all three experiments (see Figure 8 for further details).

monthly V_t's for Samoa are nearly unchanged from those calculated for 'No-Source.' In Panama, on the other hand, they increase to 0.25–0.50% during the first half of the year and to 1.25–1.55% during the second half. This very sharp increase in June coincides with the onset of the model's rainy season in Panama [*Manabe et al.*, 1974]. Note that the large excursions from the level mean are almost all positive which is consistent with the positive skewness coefficient of 1.4 calculated for the Panama series. This behavior is the result of accumulation in the boundary layer for 3–7 days, followed by sporadic ventilation that dilutes and removes the excess in the boundary layer. This process is augmented during this period by the surface flow from South and Central America, another large source region [see Figures 2 and 4 in *Levy et al.*, 1980]. During the winter and spring the prevailing winds are off the Atlantic, a nonsource region. Therefore, the air parcels passing over Panama are more uniform.

While there is currently a boundary layer monitoring program of five stations (Oregon, Samoa, Barbados, Tasmania, and Adrigal) in progress [*Cunnold et al.*, 1978], the data awaits complete analysis and is not yet available (D. M. Cunnold, private communication, 1981). Time series for Adrigal, Tasmania, and Barbados are available from the

'Swamp-Source' experiment for future comparison. It should be remembered that the model's source is idealized and not necessarily representative of the real world. Consistent with the discussion in section 1 on the current state of knowledge regarding N₂O sources and sinks, the model source distribution in 'Swamp-Source' N₂O may be appropriate for Tasmania and Adrigal, but the strength of the model source regions near Barbados might be considerably overestimated. From the model's results we conclude that a small V_t in the range of 0.1–0.2% implies that there is no significant regional source. On the other hand, near a source region we would expect to observe a much higher V_t (0.5% or greater). The actual value of V_t would depend on both the local source strength and meteorology. It should thus be clear that measuring far from tropospheric sources or sinks precludes learning much about them. It should also be noted that the model's lack of a diurnal cycle may exaggerate the degree of stagnation over land and lead, in that case, to excess variability.

5. SUMMARY AND CONCLUSIONS

Outside of the boundary layer we find that simulated tropospheric N₂O is well mixed with spatial and temporal relative standard deviations of 1% or less. Its distribution in

SIMULATED SURFACE TIME SERIES
"UNIFORM-SOURCE" N₂O

WASHINGTON
$\bar{R}$=292 ppbv
V_t=.28%

"NO-SOURCE" N₂O

WASHINGTON
$\bar{R}$=290ppbv
V_t=.17%

"SWAMP-SOURCE" N₂O
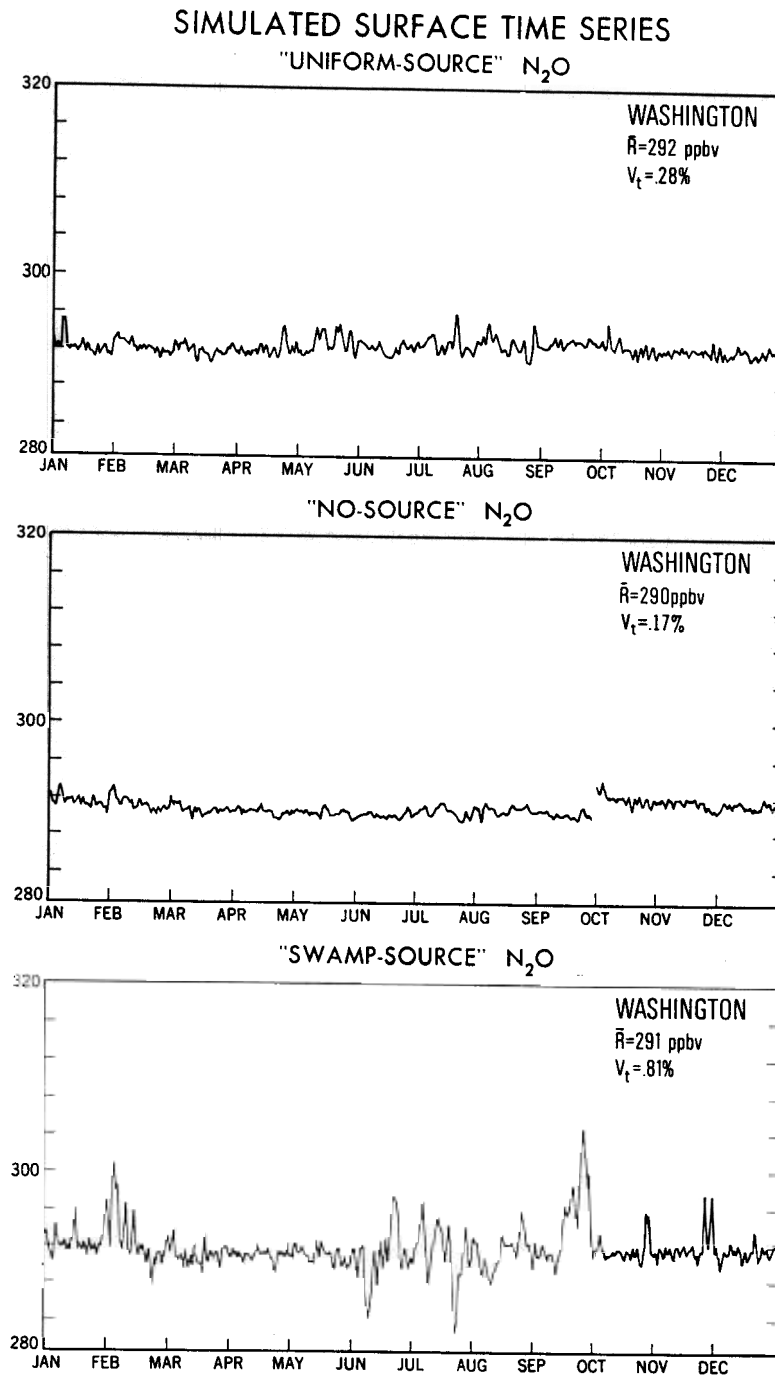

WASHINGTON
$\bar{R}$=291 ppbv
V_t=.81%

Fig. 10. One year time series (ppbv) for a surface box containing the western half of Washington (47°N, 122°W). All three experiments are presented (see Figure 8 for further details).

the middle troposphere, except for a few small regions with a cominbation of a strong surface source and strong convection, is nearly independent of the surface source's local strength and global distribution. There is a slight minimum in the northern middle and high latitudes and a broad maximum from the northern subtropics to the southern high latitudes. Very high precision north-south profiles of N₂O in the middle troposphere will be needed to determine if the model prediction of a transport induced hemispheric gradient is correct.

The boundary layer N₂O distribution is influenced by local source strength and meteorology, as well as dilution due to downward transport of N₂O poor air from the lower strato-

sphere. The north-south gradient, with a minimum in the north for the 'Uniform-Source' experiment, changes slightly in 'Swamp-Source' with the addition of an equatorial maximum. Under meteorological conditions of weak vertical transport, N₂O accumulates in the boundary layer at a rate proportional to the local source strength. In the 'Swamp-Source' experiment, some local values exceed the level average of 293 ppbv by as much as 10%. Under proper meteorological conditions (i.e., weak vertical motion and a stable boundary layer) such accumulations over source regions should be easily measured.

A more sensitive signal is given by the temporal relative standard deviation V_t. Temporal variations result from tran-
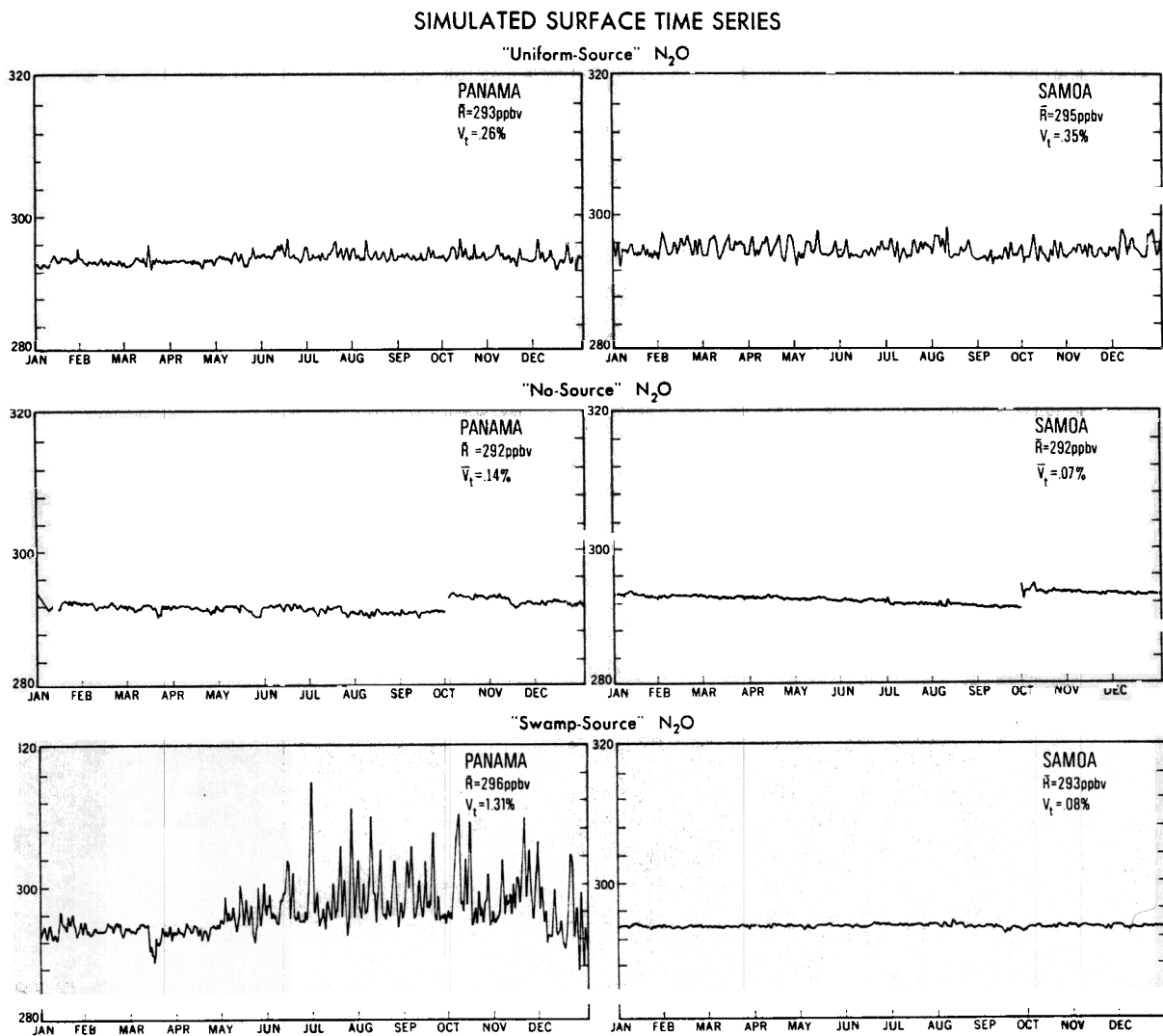
SIMULATED SURFACE TIME SERIES

Fig. 11. One year time series (ppbv) for two tropical surface boxes. Panama (9°N, 80°W) and Samoa (14°S, 171°W), for all three experiments (see Figure 8 for further details).

sient motions acting on mixing ratio gradients, both horizontal and vertical. Again, in the middle troposphere, V_t is essentially independent of both the surface source distribution and local strength. It does show some seasonal and meridional structure with $V_t \le 1\%$ from the northern subtropics to the southern polar regions and $V_t > 0.4\%$ in the northern middle and high latitudes during the winter.

In the boundary layer V_t is quite variable, even for the uniformly distributed source, with a tropical minimum of ~0.3% and northern middle and high latitude maximum >0.6%. The distribution of V_t is far from zonally symmetric with the S.H. continents having $V_t < 0.1\%$ during the summer, while in January $V_t > 0.6\%$ in the eastern equatorial Pacific. When we consider a highly nonuniform source such as 'Swamp-Source,' the V_t boundary layer field becomes much more complex. Regions far from source regions have $V_t < 0.1\%$, while in the source region we have V_t reaching 1–2% for a global source that is still small enough to balance an atmospheric lifetime of 131 years. It is incorrect to apply the empirical Junge relationship between V_t and atmosphere lifetime to measurements made in the boundary layer, as the wide range of simulated V_t values demonstrates.

The structure of the individual time series from the boundary layer depends on local source strength, distance from the local source, and the local meteorology. While it is not possible to determine the atmospheric lifetime from measured boundary layer time series, a great deal can be learned about the local sources from a combination of time series measurements and local meteorological data. One should expect to observe significant synoptic scale variability (~1%) in boundary layer N₂O time series measured in source regions.

These conclusions, while specific in this paper to N₂O, are, in fact, quite general and applicable to most long-lived tracers with surface sources and destruction in the stratosphere. An important exception would be those gases with significant anthropogenic sources whose distributions have not reached statistical equilibrium.

APPENDIX A. PARAMETERIZATION OF SUBGRID-SCALE TRANSPORTS

1. Introduction

In the set of N₂O experiments reported here, it was necessary to develop new parameterization schemes for subgrid-scale transport. Special care in choosing subgrid-

scale diffusion schemes is needed for studies concerned with tracer variability (such as this one). While diffusion is of lesser importance in the more traditional problems concerned with average tracer distributions, it plays a direct role in damping tracer variance.

Although the theoretical basis for these types of parameterizations remains limited, we believe that the most obvious mistakes can be avoided. For example, fundamental principles demand that the diffusion coefficients must be positive and of a sufficient magnitude to provide for damping of smaller-scale fluctuations that result from the stretching of tracer elements by large scale motions. On the other hand, we (and many others) have found that the 'classical' use of a constant eddy diffusion coefficient is undesirable because it is insufficiently scale selective. That is, a coefficient large enough to provide reasonable damping at the smallest spatial scales provides too much damping at larger scales. A better choice is to use a scheme which provides essentially no damping at larger scales and structure-dependent damping at smaller scales.

Such a choice has the important advantage of being rather 'passive' because the damping is produced in response to the large-scale, three-dimensional dynamics simulated by the model. Thus, even though there is a degree of arbitrariness to these (or any other) diffusion parameterizations, clever choices can 'allow' the model to determine its own tracer variability. Accordingly, we have chosen to use structure-dependent forms for the subgrid-scale diffusion coefficients as explained below.

2. Horizontal Diffusivity

The horizontal diffusivity used is a modification of the scheme developed by Mahlman and Moxim [1978]. In that study they defined the horizontal diffusion coefficient as

$$K_{H_{0,l}} = C \ (0.2\Delta S)^2 \ |D|_{0,l} \left[Q + - Q) \cdot \left| \frac{R_0 - R_l}{R_0 + R_l + \varepsilon} \right| \right]^2 \quad (A1)$$

where C and Q are unspecified dimensionless constants, S the average grid size, $|D|$ the magnitude of the horizontal velocity deformation, R_0 and R_l are mixing ratios at the central grid box (0) and its neighbor (l), respectively, and ε is a very small positive constant introduced to avoid ambiguity when R_0 and R_l are both zero. The quantity inside the absolute value brackets is a measure of the relative variability of R between two grid points. In that experiment, the values used for the constants were $C = 10$ and $Q = 0$. The conceptual and philosophical motivations for the form given by (A1) are explained in Mahlman and Moxim [1978].

Using the value $Q = O$ in (A1) for our early N₂O simulation led to some numerical difficulties. Because the variability of N₂O is so small, the value of K_H became extremely small. This small K_H had the effect of leaving tracer variations on even the smaller scales virtually undamped. As a result there was an excessive accumulation of tracer variations at the smallest resolved horizontal scales. A statistical interpretation of the problem is that the zonal spectra of squared N₂O showed unreasonable power at the highest resolved wave numbers. In fact, at the higher zonal wave numbers, the spectral slope was 'flatter' than '−1' (the limit for a freely cascading tracer in two dimensions).

After some experimentation, we found that a choice of $Q = \sqrt{0.05}$ and $C = 10$ provided sufficient damping to eliminate the grid-scale 'noise' and give a more reasonable slope of the zonal squared N₂O spectra. With these choices the value of K_H has the following properties:

High relative variability limit

$$\left[Q + (1 - Q) \cdot \left| \frac{R_0 - R_l}{R_0 + R_l + \varepsilon} \right| \right]^2 \to 1$$

$$K_{H_{0,l}} \to 10 \ (0.2\Delta S)^2 |D|_{0,l} \quad (A2a)$$

Low relative variability limit

$$\left[Q + (1 - Q) \cdot \left| \frac{R_0 - R_l}{R_0 + R_l + \varepsilon} \right| \right]^2 \to 0.05,$$

$$K_{H_{0,l}} \to 0.5 \ (0.2\Delta S)^2 |D|_{0,l} \quad (A2b)$$

These limits illustrate the degree of scale selectivity of the scheme, since the Smagorinsky [1963] subgrid-scale parameterization used in the 'parent' general circulation model [Manabe et al., 1974] uses $K_H = (0.2\Delta S)^2 |D|_{0,l}$. Thus, at low variability (the usual case) the diffusivity is 1/2 that value, while it is 10 times that value at high local variability.

3. Vertical Diffusivity

In the previous tracer experiments, the vertical subgrid-scale diffusion was set to zero. In those experiments [Mahlman and Moxim, 1978; Mahlman et al., 1980], our emphasis was on stratospheric transport. As pointed out there, we adopted the zero value to examine the capability of the explicitly resolved, large-scale motions to simulate tracer transport. For problems emphasizing tropospheric transport, a better parameterization of vertical subgrid-scale transport is required. In the troposphere a significant part of the vertical mass flux, particularly into and out of the boundary layer, occurs on scales smaller than those resolved by our grid.

As in the parameterization for horizontal diffusion, we believe that it is important to develop a scheme that is responsive to specific situations. Accordingly, we have designed a vertical diffusivity that becomes large when the flow is expected to be turbulent and small when it is inferred to be stable. This scheme is similar in overall design to that used in the GFDL 40-level GCM described by Fels et al. [1980]. That parameterization was devised to provide an adequate representation of turbulent transport processes occurring from the boundary layer to the mesopause. The scheme described below adds a crude correction for the destabilizing effect of moisture on subgrid-scale transport.

The vertical subgrid-scale momentum diffusivity is parameterized by a modified mixing length hypothesis,

$$K_{momentum} \frac{\left| \dfrac{\partial \vec{V}_2}{\partial z} \right|}{} A \cdot F \quad (A3)$$

where l_z is the mixing length (assumed to be 30 m when turbulence is occurring), $\partial \vec{V}_2 / \partial z$ the vertical wind shear magnitude, and A and F are dimensionless quantities ex-

plained below. The quantity F is a function of the moist bulk Richardson number (Ri_m):

$$F = \left(1 - 4\frac{Ri_m}{A}\right)^2 \quad \text{when} \quad 0 \leq \frac{Ri_m}{A} \leq 0.25$$

$$F = \quad \text{when} \quad \frac{Ri_m}{A} < 0 \qquad \text{(A4)}$$

$$F = 0 \quad \text{when} \quad \frac{Ri_m}{A} \geq 0.25$$

Here we define the critical value of Ri_m/A for 'turbulence onset' to be 0.25.

The moist bulk Richardson number is given by

$$Ri_m = \frac{\dfrac{g}{T}\left(\dfrac{g}{c_p} + \dfrac{\partial T}{\partial z} + \dfrac{L}{c_p}\dfrac{\partial R_{H_2O}}{\partial z}\right)}{\left|\dfrac{\partial \vec{V_2}}{\partial z}\right|^2} \qquad \text{(A5)}$$

where g is acceleration of gravity, T the temperature, c_p the specific heat of dry air at constant pressure, L the latent heat of vaporization, R_{H_2O} the mixing ratio of water vapor, and u and v the eastward and northward velocity components, respectively.

The vertical wind shear magnitude, $|\partial \vec{V_2}/\partial z|$, appears in (A3) and (A5) and is defined by

$$\left|\frac{\partial \vec{V_2}}{\partial z}\right| = \left[\left(\frac{\partial u}{\partial z}\right)^2 + \left(\frac{\partial v}{\partial z}\right)^2 + 1 \times 10^{-8}\right]^{1/2} \text{ s}^{-1} \quad \text{(A6)}$$

The constant in this expression guarantees that a finite value of Ri_m and some vertical diffusion will occur in an unstable layer that has a zero vertical wind shear.

In (A5) we have included a 'moist instability' correction to the Richardson number calculation. We do this to compensate for an important difference between this 'off-line' tracer model [Mahlman and Moxim, 1978] and a direct integration of the parent GCM [e.g., Manabe et al., 1974]. In the GCM, 'moist convective adjustment' occurs when a layer is saturated and the equivalent potential temperature decreases with height (essentially when the numerator of (A5) is negative). When such an adjustment occurs in parent GCM, heat and water vapor are mixed in the vertical so as to eliminate the instability [Manabe et al., 1965].

In the tracer model the inclusion of moisture effects in the Richardson number calculation allows a diagnosis of situations in which subgrid-scale mixing in the vertical is significantly enhanced by the release of latent heat. This is accomplished by setting $\partial R_{H_2O}/\partial z$ = 'moist saturated value' when model local precipitation is greater than 0.1 cm/6 hour and $\partial R_{H_2O}/\partial z$ = 0 when precipitation is less than 0.1 cm/6 hour.

The function 'A' is an empirically determined 'correction' to the vertical shear and to the Richardson number measured in a model grid of finite vertical thickness. This is applied to compensate for the vertical shear underestimate and the Ri overestimate when the grid size is large relative to the scale of turbulent layers. The function chosen is

$$A \equiv 1. + 0.1\left(\frac{\Delta z}{0.1}\right)^{3/2} \qquad \text{(A7)}$$

where Δz is the vertical grid size in kilometers. The choice of this function has been empirically derived from the Ri calculations of Reiter and Lester [1967] and has been checked against GCM data from the high resolution troposphere part of the GFDL model presented by Fels et al. [1980]. When the grid size is small $A \rightarrow 1$, while at $\Delta z = 3$ km, for example, $A = 17.4$.

In this parameterization we relate the heat diffusivity (K_{heat}) to the momentum diffusivity by

$$K_{\text{heat}} = K_{\text{momentum}} \cdot (0.1 + 0.9F) \qquad \text{(A8)}$$

Thus, the ratio of these two K's varies from 0.1 to 1.0 depending on the value of Ri_m. This formulation was guided by the Project HICAT analyses of turbulent fluxes in the free atmosphere [Lilly et al., 1974; Panofsky and Heck, 1974].

Normally, it is assumed that the tracer eddy diffusion coefficient (K_z) is the same as that for heat. However, in the type of model used here, it is rather easy for a tracer field to be stretched and sheared to the point where its relative variations in the vertical are large even when the fields of T, u, and v are comparatively smooth (large Ri_m). In view of this, we have found empirically that model $2\Delta z$ fluctuations are reduced when we add a small term to the vertical heat diffusivity of the form

$$K_{z_{K+1/2}} = K_{\text{heat}_{K+1/2}} + 3 \times 10^3 \text{ cm}^2 \text{ s}^{-1}\left(\frac{R_{K+1} - R_K}{R_{K+1} + R_K + \varepsilon}\right)$$

$$\text{(A9)}$$

where K is a vertical grid index. This correction is in a spirit similar to that used in the horizontal diffusivity in (A1). It has the virtue of being extremely small when the relative tracer variations are small, but as large as 3×10^3 cm^2 s^{-1} locally where the relative variations are very large [e.g., see Table 2 of Mahlman and Moxim, 1978].

The finite difference formulation of vertical diffusion follows the 'box method' rules established by Kurihara and Holloway [1967] and by Mahlman and Moxim [1978]. The method of time integration uses a simple forward explicit step that leads to computational instability when $K_z 2\Delta t/(\Delta z)^2 > 0.5$. To maintain stability, the maximum value permitted for this quantity is 0.3. Corrections back to the 0.3 limit are only required between the bottom two model levels, and then only rarely.

4. Parameter Choices for the 'High Diffusion Experiment'

As mentioned in Section 2.1, we have examined the model's sensitivity to substantial increases in the turbulent diffusivities. To evaluate this within the framework of the parameterizations developed, we have chosen to vary some of the more uncertain arbitrary parameters in the formulation.

In the horizontal diffusivity, we set $Q = \sqrt{0.2}$. At high relative variability (equation (A2a)) this gives the same value as before. At low relative variability (typical for N$_2$O), this value of Q inserted into (A2b) gives a quadrupled value of K_H.

For the vertical diffusivity, we allow the critical scaled Richardson number to be 1.0. This corresponds to the so-called 'equilibrium turbulence' limit. Accordingly, for the

'high diffusion' test we redefine (A4) to be

$$F = \left(1 - \frac{Ri_m}{A}\right)^2 \quad \text{when} \quad 0 \le \frac{Ri_m}{A} \le 1.0$$

$$F = 1 \quad \text{when} \quad \frac{Ri_m}{A} \le 0$$

$$F = 0 \quad \text{when} \quad \frac{Ri_m}{A} \ge 1.0$$

This allows for a wider range of circumstances in which vertical turbulent diffusivity is locally important. It is also possible that this 'equilibrium turbulence' limit is more appropriate, although the available information remains somewhat controversial in this regard.

APPENDIX B. CALCULATION OF N$_2$O DESTRUCTION

As long as the absorbing species' mixing ratios remain constant in a given layer, equation 3 from section 2.2 is exact regardless of thickness. However, the N$_2$O mixing ratio decreases rapidly in the middle stratosphere where the model's vertical resolution is very coarse. Therefore it was necessary to develop a parameterization that compensates for this deficiency.

In a series of off-line calculations we determined that there is no significant N$_2$O destruction below the model's second level (52.3 mbar); that a factor of 2 reduction in the Schumann-Runge band (SRB) absorption for $\lambda < 1950$ Å causes a less than 1% increase in J_4 (this is in agreement with the earlier conclusions of *Fang et al.* [1974] who found, after making detailed line-by-line calculations, that the SRB have no impact on N$_2$O photodissociation); and that 17 vertical levels over the interval 0–52.3 mbar are sufficient to give a convergent calculation of (3) and (2) in section 2. We then calculated, for a range of surface pressures and latitudes, the yearly mean values of the N$_2$O destruction rate in the top two GCM layers, 0–27.6 mbar and 27.6–52.3 mbar, with a high-resolution, 17 layer photochemical model.

The correction factors for levels 1 and 2 are defined by

$$C1 = \left(\overline{\sum_j D_j R(j)}^{\,\mathrm{yr}}\right) \Big/ \overline{D_{10\mathrm{mbar}}\, R(10\mathrm{mbar})}^{\,\mathrm{yr}}$$

$$C2 = \left(\overline{\sum_i D_i R(i)}^{\,\mathrm{yr}}\right) \Big/ \overline{D_{38\mathrm{mbar}}\, R(38\mathrm{mbar})}^{\,\mathrm{yr}}$$

where j is summed over 15 vertical levels between 0 and 27.6 mbar and i is summed over 2 between 27.6 and 52.3 mbar.

We used the initial zonally symmetric 11 level $R_{\mathrm{N_2O}}$ field for these calculations. The fine resolution profiles between 0 and 52.3 mbar were generated by linear interpolation between the values in the initial tracer field at the vertical levels 10, 38, and 65 mbar. Above 10 mbar we assumed that $R_{\mathrm{N_2O}}$ (2 mbar) $= 0.25 \cdot R_{\mathrm{N_2O}}$ (10 mbar) and that $R_{\mathrm{N_2O}}$ (1 mbar) $= 0.5 \cdot R_{\mathrm{N_2O}}$ (2 mbar). We used preliminary 1-D K_z eddy diffusion calculations and transport insights gained from previous numerical experiments to generate both the vertical profile and the north-south gradients for the initial tracer field. While, in fact, our initial $R_{\mathrm{N_2O}}$ field underestimated both the north-south gradient and the values in the

tropical stratosphere, the correction coefficients were not affected.

REFERENCES

Ackerman, M., Ultraviolet solar radiation related to mesospheric processes, in *Mesospheric Models and Related Experiments*, pp. 149–159, D. Reidel, Hingham, Mass., 1971.

Adel, A., Note on the atmospheric oxides of nitrogen, *Astrophys. J.*, *90*, 627, 1939.

Adel, A., Atmospheric nitrous oxide and the nitrogen cycle, *Science*, *113*, 624–625, 1951.

Connell, P. S., R. A. Perry, and C. J. Howard, Tunable diode laser measurements of nitrous oxide in air, *Geophys. Res. Lett.*, *7*, 1093–1096, 1980.

Crutzen, P. J., The influence of nitrogen oxides on the atmospheric ozone content, *Q. J. R. Meteorol. Soc.*, *96*, 320–325, 1970.

Crutzen, P. J., Ozone production rates in an oxygen-hydrogen-nitrogen atmosphere, *J. Geophys. Res.*, *76*, 7311–7327, 1971.

Crutzen, P. J., Upper limits on atmospheric ozone reductions following increased application of fixed nitrogen to the soil, *Geophys. Res. Lett.*, *3*, 169–172, 1976.

Cunnold, D. M., F. N. Alyea, and R. G. Prinn, A methodology for determining the atmospheric lifetime of fluorocarbons, *J. Geophys. Res.*, *83*, 5493–5500, 1978.

Fang, T. M., S. C. Wofsy, and A. Dalgarno, Opacity distribution functions and adsorption in Schumann-Runge bands of molecular oxygen, *Planet. Space Sci.*, *22*, 413–425, 1974.

Fels, S. B., J. D. Mahlman, M. D. Schwarzkopf, and R. W. Sinclair, Stratospheric sensitivity to perturbations in ozone and carbon dioxide: Radiative and dynamical response, *J. Atmos. Sci.*, *37*, 2265–2297, 1980.

Goldan, P. D., W. C. Kuster, A. L. Schmeltekopf, F. C. Fehsenfeld, and D. L. Albritton, Correction of atmospheric N$_2$O mixing-ratio data, *J. Geophys. Res.*, *86*, 5385–5386, 1981.

Hahn, J., and C. Junge, Atmospheric nitrous oxide: A critical review, *Z. Naturforsch.*, *32a*, 190–214, 1977.

Hampson, R. F., and D. Garvin, Chemical kinetic and photochemical data for modelling atmospheric chemistry, *Tech. Note 866*, Nat. Bur. of Stand., Washington, D. C., 1975.

Holloway, J. L., Jr., Smoothing and filtering of time series and space fields, in *Advances in Geophysics*, vol. 4, pp. 351–389, Academic, New York, 1958.

Johnston, H. S., and G. Selwyn, New cross section for the absorption of near ultra-violet radiation by nitrous oxide (N$_2$O), *Geophys. Res. Lett.*, *2*, 549–551, 1975.

Johnston, H. S., O. Serang, and J. Podolske, Instantaneous global nitrous oxide photochemical rates, *J. Geophys. Res.*, *84*, 5077–5082, 1979.

Junge, C. E., Residence time and variability of tropospheric trace gases, *Tellus*, *26*, 477–488, 1974.

Kurihara, Y., and J. L. Holloway, Jr., Numerical integration of a nine-level global primitive equations model formulated by the box method, *Mon. Weather Rev.*, *95*, 509–530, 1967.

Levy, H., II, Photochemistry of the troposphere, in *Advances in Photochemistry*, edited by J. N. Pitts, Jr., G. S. Hammon, and K. Gollnick, John Wiley, New York, 1974.

Levy, H., II, and J. D. Mahlman, Modeling tropospheric N$_2$O, in *Proceedings of the NATO Advanced Study Institute on Atmospheric Ozone: Its Variations and Human Influences*, edited by A. C. Aikin, pp. 893–907, Federal Aviation Administration, Washington, D. C., 1980.

Levy, H., II, J. D. Mahlman, and W. J. Moxim, A preliminary report on the numerical simulation of the three-dimensional structure and variability of atmospheric N$_2$O, *Geophys. Res. Lett.*, *6*, 155–158, 1979.

Lilly, D. K., D. E. Waco, and S. I. Adelfang, Stratospheric mixing estimated from high altitude turbulence measurements, *J. Appl. Meteorol.*, *13*, 488–493, 1974.

Liu, S. C., R. J. Cicerone, T. M. Donahue, and W. L. Chameides, Limitation of fertilizer-induced ozone reduction by the long

lifetime of the reservoir of fixed nitrogen, *Geophys. Res. Lett., 3*, 157–160, 1976.

Liu, S. C., R. J. Cicerone, T. M. Donahue, and W. L. Chameides, Sources and sinks of atmospheric N₂O and the possible ozone reduction due to industrial fixed nitrogen fertilizers, *Tellus, 29*, 251–263, 1977.

Mahlman, J. D., and W. J. Moxim, Tracer simulation using a global general circulation model: Results from a mid-latitude instantaneous source experiment, *J. Atmos. Sci., 35*, 1340–1374, 1978.

Mahlman, J. D., H. Levy II, and W. J. Moxim, Three-dimensional tracer structure and behavior as simulated in two ozone precursor experiments, *J. Atmos. Sci., 37*, 655–685, 1980.

Manabe, S., D. G. Hahn, and J. L. Holloway, Jr., The seasonal variation of the tropical circulation as simulated by a global model of the atmosphere, *J. Atmos. Sci., 31*, 43–83, 1974.

Manabe, S., J. Smagorinsky, and R. F. Strickler, Simulated climatology of a general circulation model with a hydrologic cycle, *Mon. Weather Rev., 93*, 769–798, 1965.

McElroy, M. B., Sources and sinks for nitrous oxide, in *Proceedings of the NATO Advanced Study Institute on Atmospheric Ozone: Its Variations and Human Influences*, edited by A. C. Aikin, pp. 345–364, Federal Aviation Administration, Washington, D. C., 1980.

McElroy, M. B. and J. C. McConnell, Nitrous oxide: A natural source of stratospheric NO, *J. Atmos. Sci., 28*, 1095–1098, 1971.

McElroy, M. B., S. C. Wofsy, and Y. L. Yung, The nitrogen cycle: Perturbations due to man and their impact on atmospheric N₂O and O₃, *Phil. Trans. R. Soc.*, London, Ser. A., *277*, 159–181, 1977.

McElroy, M. B., J. W. Elkins, S. C. Wofsy, and Y. L. Yung, Sources and sinks for atmospheric N₂O, *Rev. Geophys. Space Phys., 14*, 143–150, 1976.

Nicolet, M., and A. Vergison, L'Oxyde azoteux daus la stratosphere, *Aeron. Acta, 90*, 1–16, 1971.

Panofsky, H., and W. Heck, Vertical dispersion near 20 km, in

Proceedings Third Conference Climatic Impact Assessment Program, edited by A. J. Broderick and T. M. Hard, *DOT-TSC-OST-74-15*, Dep. of Transp., Washington, D. C., 1974.

Pierotti, D., and R. A. Rasmussen, Combustion as a source of nitrous oxide in the atmosphere, *J. Geophys. Res., 3*, 265–267, 1976.

Pierotti, D., and R. A. Rasmussen, The atmospheric distribution of nitrous oxide, *J. Geophys. Res., 82*, 5823–5832, 1977.

Pierotti, D., R. A. Rasmussen, and R. Chatfield, Continuous measurements of nitrous oxide in the troposphere, *Nature, 274*, 574–576, 1978.

Reiter, E. R., and P. F. Lester, The dependence of the Richardson number on scale length, *Atmos. Sci. Pap. 111*, Colorado State Univ., Fort Collins, 1967.

Selwyn, G., J. Podolske, and H. S. Johnston, Nitrous oxide ultraviolet absorption spectrum at stratospheric temperatures, *Geophys. Res. Lett., 4*, 427–430, 1977.

Simon, P., Balloon measurements of solar fluxes between 1960 Å and 2300 Å in Proceedings Third Conference on Climatic Impact Assessment Program, edited by A. J. Broderick and T. Hard, *DOT-TSC-OST-74-15*, Dep. of Transp., Washington, D. C., 1974.

Singh, H. B., L. J. Salas, and H. Shigeishi, The distribution of nitrous oxide (N₂O) in the global atmosphere and the Pacific Ocean, *Tellus, 31*, 313–320, 1979.

Smagorinsky, J., General circulation experiments with the primitive equations, *Mon. Weather Rev., 91*, 99–164, 1963.

Weiss, R. F., The temporal and spatial distribution of tropospheric nitrous oxide, *J. Geophys. Res., 86*, 7185–7195, 1981.

Weiss, R. F., and H. Craig, Production of atmospheric nitrous oxide by combustion, *Geophys. Res. Lett., 3*, 751–753, 1976.